ESD-TR-75-205

Semiannual Technical Summary

Seismic Discrimination

30 June 1975

Prepared for the Advanced Research Projects Agency
under Electronic Systems Division Contract F19628-73-C-0002 by

Lincoln Laboratory

MASSACHUSETTS INSTITUTE OF TECHNOLOGY

LEXINGTON, MASSACHUSETTS

The work reported in this document was performed at Lincoln Laboratory, a center for research operated by Massachusetts Institute of Technology. This research is a part of Project Vela Uniform, which is sponsored by the Advanced Research Projects Agency of the Department of Defense under Air Force Contract F19628-73-C-0002 (ARPA Order 512).

This technical report has been reviewed and is approved for publication.

FOR THE COMMANDER

Eugene C. Raabe

Eugene C. Raabe, Lt. Col., USAF
Chief, ESD Lincoln Laboratory Project Office

MASSACHUSETTS INSTITUTE OF TECHNOLOGY
LINCOLN LABORATORY

SEISMIC DISCRIMINATION

SEMIANNUAL TECHNICAL SUMMARY REPORT TO THE ADVANCED RESEARCH PROJECTS AGENCY

1 JANUARY – 30 JUNE 1975

ISSUED 15 AUGUST 1975

LEXINGTON MASSACHUSETTS

ABSTRACT

This report describes 23 investigations in the field of seismic discrimination. These are grouped as follows: seismic body wave studies (3 contributions), seismic surface wave studies (5 contributions), investigations of seismic source mechanisms (2 contributions), studies of earth heterogeneity and scattering phenomena (5 contributions), studies of earthquake occurrence rates (3 contributions), and outlines of progress in seismic data management system development and improvements in in-house computer facilities (5 contributions).

CONTENTS

SUMMARY

This is the twenty-third Semiannual Technical Summary report describing the activities of Lincoln Laboratory, M.I.T., in the field of seismic discrimination. These activities involve research into the fundamental seismological problems associated with the detection, location, and identification of earthquakes and nuclear explosions. We also are concerned with the development of methods for the handling and analysis of large quantities of global seismic data, and the application of these methods to data management system design and the optimum extraction of scientific information from high-quality digital data.

Several investigations in the general area of seismic body waves are described. We are continuing to develop the application of maximum entropy cepstral analysis to the detection of pP-phases for explosions. Delay times estimated by this method agree very well with published shot depths and surface accelerogram recordings. An attempt has been made to verify seismic reciprocity for short-period earthquake data, as a background to the problem of calibration of aseismic areas in a threshold test treaty situation. Results are encouraging, but a residual amplitude variation by a factor of 2 (0.3 m_b units) remains unexplained. In another study, a new improved method for the calculation of ellipticity corrections is described.

In the area of surface wave studies, we have extended previous work on surface wave propagation in Eurasia. We describe the first results from an extensive attempt to use existing crustal structure information to predict surface wave path refraction and multipathing effects. Some large deviations are predicted. In another study, the source mechanisms of some Hindu Kush earthquakes have been estimated from the joint analysis of spectra from earthquake pairs. An earth flattening correction for Rayleigh-wave dispersion at long periods has been developed from normal mode theory, and seems applicable to a wide variety of structures. Another interesting development from free oscillation theory is the possibility of representing surface wave sources in a moment tensor formalism. This would appear to be advantageous for seismic discrimination problems. A new approach to the estimation of path corrections for surface wave magnitudes has been tested using data for the Cannikin explosion. Only limited improvement over existing techniques has been demonstrated so far.

Earlier work on the determination of seismic source parameters from long- and short-period P-waveforms has been continued. Considerable success has been obtained using long-period information, and it is clear that there is considerable source information in the short-period waveforms, though propagation effects make it hard to extract in some cases. An interesting application of source mechanism discrimination by a multi-parameter approach is described. Earthquakes on the mid-Atlantic ridge can be separated into dip-slip (ridge) and strike-slip (transform) types with a high level of success.

Research into earth heterogeneity and path effects has concentrated on two areas — the inversion of P-wave travel-time residuals to obtain lateral variations in structure, and the further study of the scattering of seismic waves. The first results from a global analysis of 728,072 observations of P and PKIKP are presented. Third-order spherical harmonic analysis indicates significant correlations between inhomogeneities at different levels in the mantle. Inversion of travel-time observations at NORSAR shows evidence of pipe-like structures that extend below the Mohorovicic discontinuity. Polarization studies of the short-period arrivals at the three-component site at LASA show a surprisingly complex coda which is a strong function of source location. The locations of the scatterers are being investigated. A theoretical study of primary

scattering by a transition zone of changing velocity is outlined. New attempts to characterize the scattering processes beneath large arrays are described.

We are continuing investigations into the properties of earthquake time series, formed by counts of earthquakes above a given magnitude threshold per unit time. Significant correlations between the time series for widely separated regions of various tectonic types are found. This strongly suggests the presence of a global earthquake triggering mechanism. Spectral analysis has been applied to the regional earthquake time series, using the maximum entropy method, and approximately 30 percent of the energy in the spectrum are found to correlate across all regions. A spectral peak at a 6-month period is presumably due to earth tides. Another at 7.6 months remains unexplained.

We are deeply involved in the design and development of the data management system for the proposed ARPA seismic network. In particular, we have been experimenting with a documentation system for the network, based on the On-Line System (NLS) developed by Stanford Research Institute. Creation of file structures and input of documentation are progressing. An attempt to access filed information on the datacomputer is described.

We continue to update and modify our in-house computer systems so that we can take full advantage of the new digital seismic data as they become available on the datacomputer. Some recent improvements and progress are reported.

M. A. Chinnery

GLOSSARY

ARPA	Defense Advanced Research Projects Agency
ARPANET	ARPA Computer Network
ASG	Applied Seismology Group
BBN	Bolt Beranek & Newman
BMEM	Burg Maximum Entropy Method
CCA	Computer Corporation of America
CPU	Central Processing Unit
CRT	Cathode Ray Tube
DADS	Data Analysis and Display System
DDC	Defense Documentation Center
DU	Data Unit
HGLP	High Gain Long Period
ISC	International Seismological Center
IWWSS	Integrated World-Wide Seismic System
LASA	Large Aperture Seismic Array
NEIS	National Earthquake Information Service
NLS	On-Line System
NORSAR	Norwegian Seismic Array
PDE	Preliminary Determination of Epicenters
PEM	Parametric Earth Model
SATS	Semiannual Technical Summary
SRO	Seismic Research Observatory
TENEX	PDP-10 Operating System
USGS	United States Geological Survey
WWSSN	World-Wide Standard Seismograph Network

SEISMIC DISCRIMINATION

1. BODY WAVE STUDIES

A. MAXIMUM ENTROPY CEPSTRAL ANALYSIS

The Maximum Entropy Cepstral Analysis method[1] has been evaluated by determining the delay time between the P- and pP-phases in short-period seismograms recorded at Norway for seven Nevada Test Site explosions and comparing the results to the observed times determined from ground zero accelerograms.[2] Table I-1 is a list of the events and includes the observed delay time and the calculated times of the primary cepstral peak (T_{CALC}) and first harmonic divided by 2 (T^2_{CALC}) (when it was observed). The data were recorded at 10 Hz and the cepstra were read to the nearest 0.05 sec.

TABLE I-1
CALCULATED AND OBSERVED DELAY TIMES FOR NTS EVENTS

Date	Origin Time	Event Name	Depth (m)	T_{pP-P} (observed) (sec)	T_{CALC} (T^2_{CALC}) (sec)
7-16-69	1455:00	Hutch	549	0.59	0.45 (0.50)
6-9-68	1400:00	Noggin	582	0.75	0.55
3-22-68	1500:00	Stinger	668	0.85	0.90 (0.85)
10-18-67	1430:00	Lanphere	715	0.86	0.75 (0.80)
1-19-68	1815:00	Faultless	975	0.80	0.70 (0.70)
4-26-68	1500:00	Boxcar	1158	0.96	0.95 (0.95)
3-26-70	1900:00	Handley	1207	0.95	1.10

Figure I-1 plots the results. The observed and calculated times agree to within one or two digitizing intervals. Peaks due to spall closure[2] were not observed or possibly were unresolvable from the peak due to the first harmonic of the depth phase echo. Since the existence of a cepstral peak due to an echo depends on the echo and primary having essentially the same shape, it is not surprising that the peak due to the surface-spall closure phase is not present.

To further evaluate the method, the short-period LASA recording of a presumed explosion from Eastern Kazakh (m_b = 5.5, Δ = 83°) was analyzed. Figure 1-2 shows the seismogram and the maximum entropy cepstrum indicating a pP-P delay time of 0.41 sec. Again, no indication of an echo due to spalling is observed.

The results presented here indicate that the technique gives accurate estimates of the pP-P delay time for explosions based on teleseismic recordings. Work is continuing to determine the magnitude threshold and minimum delay time for which reliable estimates can be obtained.

T. E. Landers

B. TEST OF SHORT-PERIOD RECIPROCITY

Will a force F applied at point P in the real earth, which produces a short-period transient displacement U at point Q, produce the same displacement U at P when applied at Q? This question bears on the feasibility of calibrating certain short-period paths in a threshold test treaty. We have performed an experiment which attempts to answer the question stated above for a specific path.

We searched a ten-year earthquake list to find two large shallow earthquakes near WWSSN stations within 30° to 90° of each other. It developed that only one set of station-event pairs was found suitable for the experiment, namely:

Event	Near	Recorded at
20 Jan 1970 04h 45m 00.2s 8.8°N 79.2°W 33 km deep, 5.6 m_b, 5.6 M_s	Balboa Heights, Panama BHP, 8.97°N 79.56°W	Antofagasta, Chile ANT, 23.71°S 70.43°W
4 Dec 1969 17h 08m 48.7s 23.1°S 70.1°W 36 km deep, 5.9 m_b, 6.3 M_s	Antofagasta, Chile ANT	Balboa Heights, Panama BHP

Using long-period P-waves, and a procedure discussed in Sec. III-A when applied to shallow Asian earthquakes, source parameters for each of these earthquakes were estimated. This is not a unique process, but the source parameters gained are consistent with the long-period data observed in the distance range 30° to 90°. We then used these source parameters to generate a short-period, north-south seismogram at BHP from the Chilean earthquake, and the same type of record at ANT from the Panamanian earthquake. We could not compare the vertical components in this case since this record at ANT from the Panamanian earthquake is uninterpretable. Because of the north-south alignment of the path considered, the north-south components are only 15° off the radial vector between the two sites.

Figure I-3 shows the comparison between the observed and synthetic records at BHP and ANT for the events in Chile and Panama, respectively. Although different source parameters were used to generate the synthetics, the same spreading factor and attenuation operator were applied to both. The general form of the synthetics is similar to the observed data in both cases; however, the amplitude of the synthetic at ANT is about one-half that of the observed. Since the means employed here are somewhat indirect, estimating source parameters in order to scale the amplitudes, it is difficult to say whether short-period reciprocity failed by a factor of two or our ability to test the question by this means is no more accurate than a factor of two. The similarity of the form of the observed and synthetic seismograms in Fig. I-3 is, however, encouraging.

J. R. Filson
R. G. North

C. NEW METHOD OF CALCULATION OF ELLIPTICITY CORRECTIONS

The current usage of ellipticity corrections requires either extensive tables[3] in which the corrections are listed as functions of colatitude of the source, epicentral distance, and the azimuth, or an approximate formula[4] that may lead to errors as large as 0.3 sec for the P-phase.

The simple transformation, invoking the addition theorem for Legendre polynomials, of Eq. (10.30) of Bullen[5] leads to separation of variables:

$$(\tfrac{1}{3} - \cos^2\Theta') = -\tfrac{2}{3} P_2^o(\cos\Theta') = -\tfrac{2}{3} \sum_{m=0}^{2} P_{2,m}(\cos\Theta_o)\, P_{2,m}(\cos\Theta) \cos m\xi \qquad \text{(I-1)}$$

where Θ_o is the colatitude of the source, and ξ is the azimuth from the source to the epicenter; $P_{2,m}$ are defined:

$$P_{2,m} = [\epsilon_m \frac{(2-m)!}{(2+m)!}]^{1/2} P_2^m \quad ; \quad \epsilon_o = 1 \quad , \quad \epsilon_m = 2 \text{ for } m > 0.$$

Thus, the correction can be sought in a form

$$\delta t = \sum_{m=0}^{2} \tau_m(\Delta) \cdot P_{2,m}(\cos\Theta_o) \cos m\xi \quad . \qquad \text{(I-2)}$$

The efficiency of this scheme lies in the fact that only three integrals such as Eq. (10.30) of Bullen[5] need to be evaluated for a given epicentral distance and species of ray.

We have investigated the dependence of $\tau_m(\Delta)$ on the adopted earth model; two models were tested: 1066A (Ref. 6) and PEM (parametric earth model).[7] Model 1066A is characterized by continuous variation of the velocities and density in the upper mantle, while model PEM has two first-order discontinuities at depths of 420 and 670 km. Results for rays penetrating deeper than 670 km show that the difference in $\tau_m(\Delta)$ for the two models is not more than 0.01 sec for P. Since the two models are thought to represent two extremes in modeling the upper mantle, we conclude that it is very unlikely that any other acceptable model will yield significantly different values of $\tau_m(\Delta)$.

Figure I-4 shows plots of $\tau_m(\Delta)$ for the P-phase computed for surface focus and a source at 650 km depth. It has been commonly assumed that the effect of the focal depth on ellipticity correction is negligible; yet, in most unfavorable circumstances it could amount to 0.3 sec for the deep focus earthquakes.

We also examine the errors that could be introduced by application of the approximate formula of Bullen,[4]

$$\delta t = (H + h) \cdot f(\Delta) \quad .$$

Substituting

$$H = -\tfrac{2}{3} \epsilon_o a P_{2,o}(\cos\Theta_o)$$

and

$$h = -\tfrac{2}{3} \epsilon_o a \sum_{m=0}^{2} P_{2,m}(\cos\Theta_o) \cdot P_{2,m}(\cos\Delta) \cdot \cos m\xi$$

we find equivalent functions $\tau_m(\Delta)$. In Fig. I-5, we compare $\tau_m(\Delta)$ obtained using the table of $f(\Delta)$ of Jeffreys and Bullen[8] with our computations. The errors may amount easily to 0.3 sec.

The explicit formula for δt is:

$$\delta t = \tfrac{1}{2} \tau_o(\Delta)\,(3\cos^2\Theta_o - 1) + \sqrt{3}\,\tau_1(\Delta) \sin\Theta_o \cos\Theta_o \cos\xi$$

$$+ \sqrt{3}\,\tau_2(\Delta) \sin^2\Theta_o (\cos^2\xi - \tfrac{1}{2}) \quad .$$

All the trigonometric functions in this formula are automatically computed in the earthquake location routine.

Dziewonski and Gilbert[9] give tables of $\tau_m(\Delta)$ for eight seismic phases (P, PcP, PKP1, PKP2, PKIKP, S, ScS, and SKS) and three focal depths: surface, 300 km, and 650 km.

A. M. Dziewonski
F. Gilbert†

REFERENCES

1. Seismic Discrimination SATS, Lincoln Laboratory, M.I.T. (31 December 1974), DDC AD-A006194.
2. D. L. Springer, "Secondary Sources of Seismic Waves from Underground Nuclear Explosions," Bull. Seismol. Soc. Am. 64, 581-594 (1974).
3. K. E. Bullen, "The Ellipticity Correction to Travel Times in P and S Earthquake Waves," Mon. Not. R. Astron. Soc., Geophys. Suppl. 4, 143-157 (1937).
4. K. E. Bullen, "A Suggested New 'Seismological' Latitude," Mon. Not. R. Astron. Soc., Geophys. Suppl. 4, 158-163 (1937).
5. K. E. Bullen, Introduction to the Theory of Seismology, 3rd Edition (Cambridge University Press, London, 1965).
6. F. Gilbert and A. M. Dziewonski, "An Application of Normal Mode Theory to the Retrieval of Structural Parameters and Source Mechanisms from Seismic Spectra," Philos. Trans. R. Soc. Lond. A278, 187-269 (1975).
7. A. M. Dziewonski, A. L. Hales, and E. R. Lapwood, "Parametrically Simple Earth Models Consistent with Geophysical Data," Phys. Earth Planet. Inter. 10, 12-48 (1975).
8. H. Jeffreys and K. E. Bullen, Seismological Tables (British Association for the Advancement of Science, London, 1967).
9. A. M Dziewonski and F Gilbert, "The Effect of Small Aspherical Perturbations on Travel Times and Reexamination of Ellipticity," Geophys. J. R. Astron. Soc. (in press, 1975).

† Institute of Geophysics and Planetary Physics, University of California, San Diego; La Jolla, California 92037.

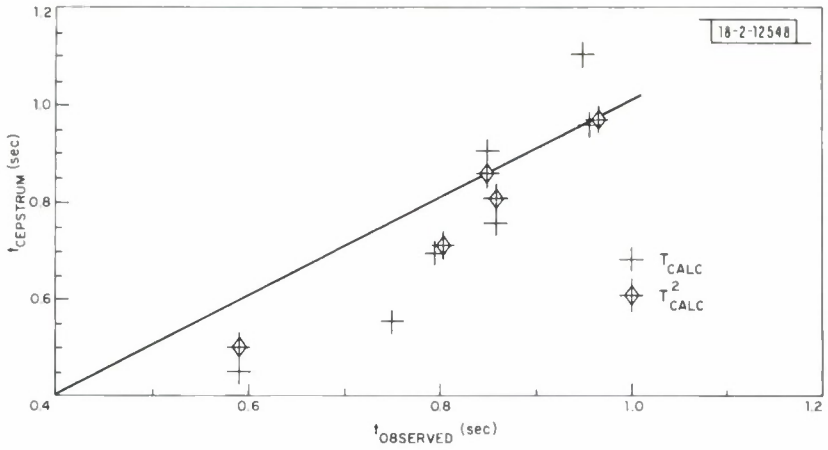

Fig. I-1. Observed vs calculated pP-P delay times.

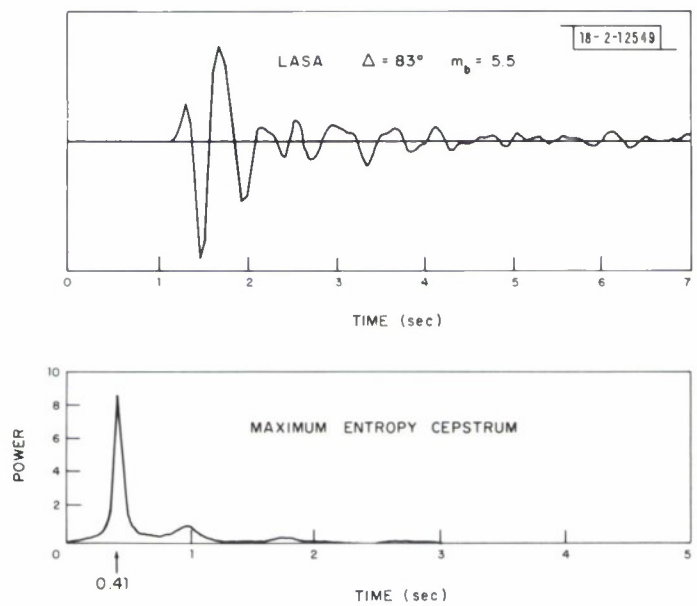

Fig. I-2. Short-period seismogram and maximum entropy complex cepstrum for presumed Eastern Kazakh explosion.

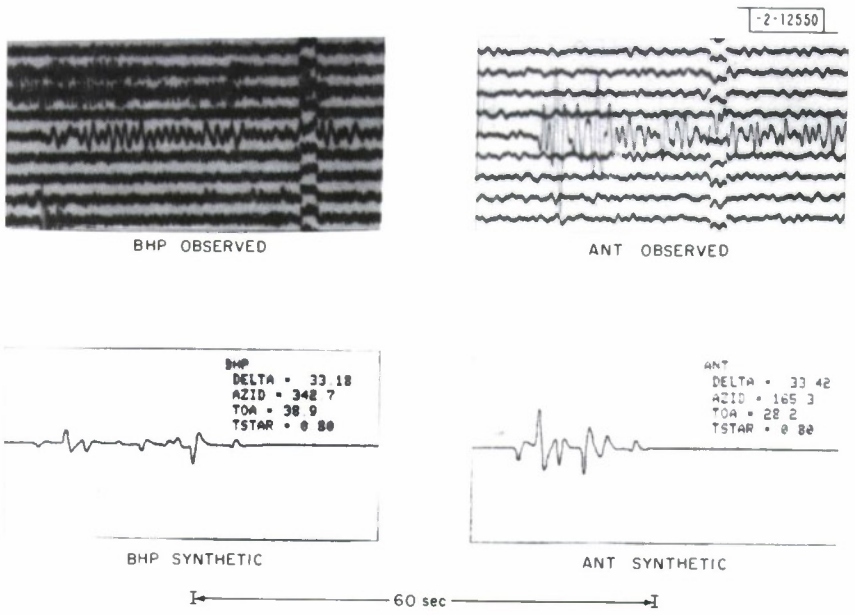

Fig. I-3. Observed and synthetic short-period, north-south seismograms at BHP (Panama) from earthquake in Chile (left) and at ANT (Chile) from earthquake in Panama (right).

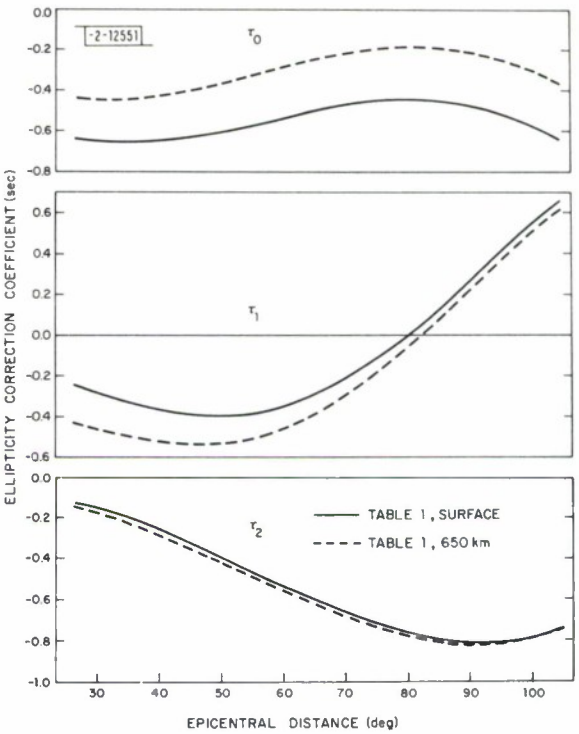

Fig. I-4. Comparison of P-phase ellipticity correction coefficients computed for focal depths: surface and 650 km.

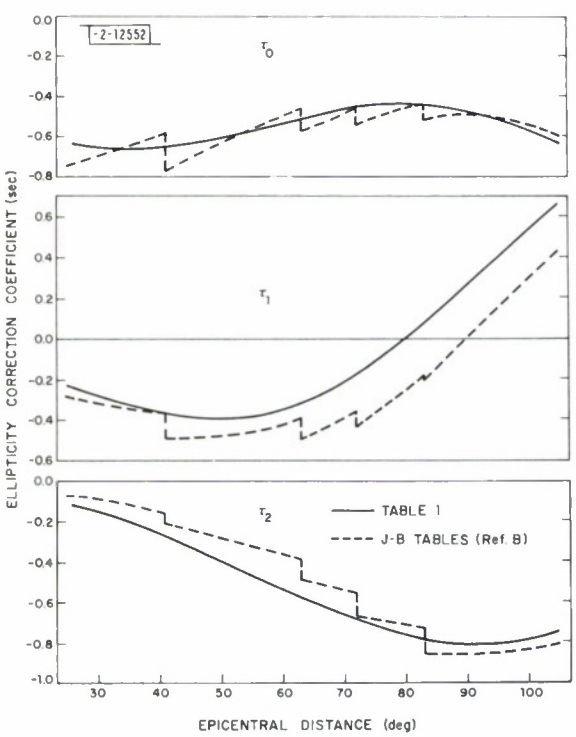

Fig. I-5. Comparison of P-phase ellipticity corrections obtained using our method of calculation $\tau_m(\Delta)$ and equivalent values for Bullen's[4] approximation: surface focus.

II. SURFACE WAVE STUDIES

A. SURFACE WAVE RAY TRACING ACROSS EURASIA

Studies of Rayleigh-wave multipath propagation using ray tracing have been reported for Western North America and the North America – Pacific boundary by B. R. Julian in previous SATS.[1] This work is now being extended to include the effects of lateral variations in structure, particularly those of major mountain ranges such as the Alps and Himalayas, upon the transmission of surface waves across Eurasia.

Information on the crustal structure of this region is considerably sparser than for North America. With the exceptions of Western Europe, European Russia, and the Soviet Far East, not much seismic refraction work has been carried out across this vast area. We therefore decided to consider initially only the effect of variation of crustal thickness upon the Rayleigh-wave dispersion. The primary source of this information, a contour map of Moho depth in Eastern Europe, the Soviet Union, and China,[2] is based (outside the regions for which refraction data are available) mainly upon elevation with occasional constraints from gravity observations. This was supplemented by similar contour maps for Scandinavia, Western Europe, and India. No data were available for Spain, Pakistan, Afghanistan, Iran, the Middle East, and Southeast Asia. The area used, however, constitutes some 75 to 80 percent of the Eurasian land mass as well as most of the adjacent continental shelf. These contour maps have been digitized at 0.5° intervals of latitude and longitude, and the resulting grid converted to one of phase velocity.

The earth model chosen for the dispersion consists of a crustal structure determined for the Alps from dispersion data,[3] and an upper-mantle model calculated to satisfy observed normal mode eigenperiods and average continental surface wave dispersion.[4] The effect of crustal thickness has been approximated by linearly expanding the crustal layers and determining the dispersion of the resultant model. Figure II-1 shows the phase velocity at 20- and 40-sec periods for Rayleigh waves as a function of crustal thickness. The values of phase velocity at these periods for a 35-km-thick crust are close to those observed for some Eurasian paths. The phase velocities can be seen to increase to nearly oceanic values as the crust becomes thinner and to decrease quite substantially as the thickness approaches the values of 50 to 75 km estimated for the Alps and Himalayas.

Considerable azimuthal anomalies have been observed at NORSAR for 20- and 40-sec period Rayleigh waves,[5] and, in an attempt to explain those observed for Eurasian events, rays have been traced through the grid at 5° increments from 45° to 225° azimuth. Figures II-2 and II-3 show the results of this ray tracing at a 20-sec period on an azimuthal equidistant projection centered at NORSAR: this projection has the advantage that all great circle paths through the center are straight lines. The rays terminate at the edge of the grid. Unfortunately, because of a lack of data for some parts of the Arctic Ocean, rays cannot be traced to the Kuriles and Japan. These figures show clearly the effect of the Alpine, Himalayan, and Central Asian fold belts upon surface wave propagation, as well as that of crustal thinning in continental shelf regions. The number at the end of each ray denotes the final azimuthal deviation suffered.

Figure II-2 shows ray paths traced at 5° from 45° to 120° azimuth from NORSAR. It can be seen that rays at azimuths up to 75° experience positive deviations; the ray at 80° is remarkably straight. In the Himalayas and Tibet (85° to 105° azimuth), the deviations vary considerably, leading to multipathing. These results may be compared with those measured using high-resolution frequency-wavenumber analysis of surface wave arrivals at NORSAR.[5] Positive

(clockwise) deviations of rays traced from NORSAR imply negative azimuthal anomalies for rays from an event to NORSAR and vice versa.

An event in Taiwan (distance 59°, azimuth 81°) had arrivals with azimuth anomalies of about +10°: this is unfortunately opposite to those shown. An event in Central Russia in the same direction gave a similar anomaly, but later arrivals had negative values which are more in agreement with those predicted. Early arrivals from events in the Hindu Kush (45°, 90°) and in Tibet (59°, 81°) came in with small negative anomalies; later ones were highly positive. The model predicts both these effects, though the deviations are about a factor of 2 to 3 times less than the observed anomalies. The velocity model evidently needs considerable refinement to produce the very high values observed.

Figure II-3 shows rays traced at 5° increments from 125° to 225° azimuth from NORSAR. Although crustal thicknesses in the Alps approach those for the Himalayas, the effect is not as marked, primarily because the Alps run normal to the ray paths in most cases. The effect of the Carpathians is somewhat greater, and it can be seen that there is considerable divergence of the ray paths in the Balkans. This should result in higher-than-average surface wave amplitudes at NORSAR for events in the Aegean and Western Turkey: a hypothesis which we hope to verify by observation. Fairly large deviations also occur around the coast of Denmark. Measurements of arrival azimuth for surface waves approaching NORSAR from the south show fairly large deviations, attributed to refraction at the coastline of North Africa.[5] The present results indicate that at least part of this (up to 15° deviation) may be caused by refraction at structures within 20° distance from NORSAR.

This study is going to be extended to include variations in crustal structure, and we hope that this will help to explain the much larger deviations observed. A division into shields, platforms, and foldbelts should give greater variations in phase velocities. The Caspian and Black Seas are believed to contain fragments of oceanic crust, and inclusion of such features should produce similar variations. An extension of the area studied to oceanic regions may be fairly easy since there seem to be simple relations between age zones and spreading rates, and lithospheric thickness, sedimentary cover, and water depth. By summing the group delay along the ray path, it also should be possible to predict the arrival time of each refracted wave.

R. G. North

B. AN EMPIRICAL EARTH FLATTENING CORRECTION FOR RAYLEIGH-WAVE DISPERSION

Calculations of dispersion curves for a layered half-space using Haskell's[6] approach are simpler, faster, and require less computer memory than computations for the spherical, gravitating earth. For the Love waves, Gerver and Kazhdan[7] and Biswas and Knopoff[8] proposed an exact earth flattening transformation. A similar transformation for Rayleigh waves is much more difficult, if not impossible, to achieve. Bolt and Dorman[9] derived an empirical formula for correcting the Rayleigh-wave phase velocities obtained for a flat earth model, and their formula commonly has been used for the last 10 to 15 years. Because of the progress in the precision and stability of the numerical solutions to the normal mode problem,[10] we decided to reexamine the question of the earth flattening correction.

We have used an oceanic (PEM-O) and a continental (PEM-C) model of the earth.[4] These models satisfy, in the sense of a weighted average, the observed periods of free oscillations and typical surface wave dispersion for each type of region. Both models are identical below 420 km

depth. As the flat earth program requires a discrete layered representation of the earth, we have introduced appropriate modifications in the PEM models.

The spherical earth normal mode eigenfrequencies ${}_0\omega_\ell$ are computed with and without consideration of gravity for the modes ${}_0S_\ell$ (Rayleigh wave). The phase velocity for a spherical earth is

$$C_s = a \cdot {}_0\omega_\ell/(1 + 1/2)$$

a being the radius of the earth. The phase velocities in a flat layered half-space C_f have been computed at frequencies ${}_0\omega_\ell$ using a program based on a layer matrix formulation.[6] Results obtained using this program agree to the published accuracy (usually 5 to 6 significant figures) with those of other matrix algorithms[11] and also with those of a program based on a numerical integration method.[12]

Consideration of gravity in the normal mode solutions has the effect of increasing the phase velocity. This increase is 0.0002 km/sec at the 50-sec period, rising to 0.0032 km/sec at 150 sec and to 0.021 at the 300-sec period. As the effect of gravity is only 0.005 percent at 50 sec, calculations for shorter periods are carried out for a nongravitating earth. In general, the effect of gravity in the period range considered is an order of magnitude less than that of sphericity: at 300 sec $\delta C = C_s - C_f$ is 0.24 km/sec; for the continental model δC is still as large as 0.01 km/sec at the 25-sec period, and for the oceanic model this difference extends to periods as short as 15 sec.

In Fig. II-4, a plot of $\delta C/T$ (division by period for scaling purposes) shows a variation which in shape resembles much more closely the group velocity variation (chain line) than the phase velocity curve (broken line). Like the group velocity curves $\delta C/T$ possesses a short-period maximum and a long-period minimum, although the minima do not coincide precisely.

The line $0.00016 \cdot C_f$ is equivalent to the Bolt-Dorman[9] correction. Having noted the similarity between $\delta C/T$ and u_f, we determine the proportionality factor:

$$\alpha_u = (C_s - C_f)/(u_f \cdot T) \quad .$$

For the continental model, the best fitting value of α_u is 0.000156, and for the oceanic structure it is 0.000166; the mean of the two (0.000162) still provides a reasonably good fit.

In Fig. II-5, we compare errors associated with our empirical correction ($\delta C = \alpha_u \cdot u_f \cdot T$) with that of Bolt and Dorman.[9] For both formulas, the errors are very small for periods less than 100 sec; this means that systematic bias introduced by application of either of the two empirical corrections is insignificant in comparison with measurement errors. Above 100 sec, however, the advantage of using $\delta C = \alpha_u \cdot u_f \cdot T$ is distinct; it predicts the exact values of C_s to within 0.2 percent (less than 0.01 km/sec) to periods as long as 230 sec, which is the approximate upper limit of the minor arc measurements of surface wave dispersion.

Since the same value of α_u fits the two quite different models fairly well, it seems that the above relation will be a good approximation for a wide variety of structures.

R. G. North
A. M. Dziewonski

C. MOMENT TENSOR REPRESENTATION OF SURFACE WAVE SOURCES

The usual equations for Love and Rayleigh waves due to a point source in a layered elastic half-space (e.g., Saito[12]) can be expressed as a linear combination of the moment tensor elements. The advantages of such an approach are (1) that the expansion is linear and therefore amenable to the stochastic least-squares estimation procedure (Foster[13]), and (2) that the expansion is complete consisting of monopole, dipole, and quadrupole terms (Knopoff and Randall[14]) which ensures reliability in the estimated source parameters. An easy way to prove this expansion is to merge the moment tensor formalism of Gilbert[15] with the vector harmonic expressions given by Saito.[12]

The Love and Rayleigh wave problems separate out onto vector components when written in terms of the vector cylindrical harmonics. These are:

$$\overrightarrow{R_m^1}(kr,\varphi) \equiv Y_m(kr,\varphi)\,\hat{z} = (0,\,0,\,Y_m)$$

$$\overrightarrow{R_m^2}(kr,\varphi) \equiv \frac{1}{k}\,\nabla Y_m(kr,\varphi) = \left(\frac{\partial Y_m}{\partial(kr)} \quad , \quad \frac{1}{kr}\,\frac{\partial Y_m}{\partial\varphi} \quad , \quad 0\right)$$

$$\overrightarrow{L_m}(kr,\varphi) \equiv \frac{1}{k}\,\nabla \times R_m^1(kr,\varphi) = \left(\frac{1}{kr}\,\frac{\partial Y_m}{\partial\varphi} \quad , \quad -\frac{\partial Y_m}{\partial(kr)} \quad , \quad 0\right)$$

$$\overrightarrow{R^2} = \hat{z} \times \vec{L} \qquad \vec{L} = \overrightarrow{R^2} \times \hat{z}$$

$$(\nabla^2 + k^2)\,Y_m(kr,\varphi) = 0$$

$$Y_m(kr,\varphi) = H_m^+(kr)\,e^{im\varphi} \tag{II-1}$$

where H_m^+ is the outward traveling Hankel wave function. The expansion becomes:

$$\vec{s}(r,z,\varphi,t) = \int_{-\infty}^{+\infty} d\omega\, e^{i\omega t} \int_0^{\infty} kdk \sum_{m=-\infty}^{+\infty} \Big[l(\omega,k,m,z)\,\overrightarrow{L_m}(kr,\varphi) + r_1(\omega,k,m,z)\,\overrightarrow{R_m^1}(kr,\varphi) + r_2(\omega,k,m,z)\,\overrightarrow{R_m^2}(kr,\varphi)\Big] \tag{II-2}$$

where the expansion coefficients l, r_1, and r_2 are solutions to the well-known Love and Rayleigh wave equations:

$$\frac{d}{dz}\begin{bmatrix} l \\ \\ T_l \end{bmatrix} = \begin{bmatrix} 0 & \frac{1}{\mu} \\ \\ \mu k^2 - \rho\omega^2 & 0 \end{bmatrix} \begin{bmatrix} l \\ \\ T_l \end{bmatrix}$$

$$T_l \equiv \mu\,\frac{dl}{dz}$$

$$T_l = 0 \qquad \text{at } z = 0$$

$$|l| \to 0 \qquad \text{as } z \to \infty$$

$$\frac{d}{dz}\begin{bmatrix} r_2 \\ r_1 \\ T_r^2 \\ T_r^1 \end{bmatrix} = \begin{bmatrix} 0 & -k & \frac{1}{\mu} & 0 \\ \frac{k\lambda}{\lambda + 2\mu} & 0 & 0 & \frac{1}{\lambda + 2\mu} \\ -\rho\omega^2 + 4k^2\mu\,\frac{(\lambda + \mu)}{(\lambda + 2\mu)} & 0 & 0 & \frac{-k\lambda}{\lambda + 2\mu} \\ 0 & -\rho\omega^2 & k & 0 \end{bmatrix} \begin{bmatrix} r_2 \\ r_1 \\ T_r^2 \\ T_r^1 \end{bmatrix}$$

$$T_r^1 \equiv (\lambda + 2\mu)\,\frac{dr_1}{dz} - k\lambda r_2 \qquad T_r^2 \equiv \mu\left(kr_1 + \frac{dr_2}{dz}\right)$$

$$T_r^1,\ T_r^2 = 0 \qquad \text{at } z = 0$$

$$|r_1|,\ |r_2| \to 0 \qquad \text{as } z \to \infty \quad . \tag{II-3}$$

Introducing expansion weights a_j and b_j allows the expansion to be written:

$$\vec{s}(r, z, \varphi, t) = \int_{-\infty}^{+\infty} d\omega\, e^{i\omega t} \int_0^{\infty} kdk \sum_{m=-\infty}^{+\infty} \left\{ \sum_j a_j(\omega, k, m)\, l(\omega_j, k, z)\, \overrightarrow{L_m}(kr, \varphi) \right.$$

$$\left. + \sum_j b_j(\omega, k, m) \left[r_1(\omega_j, k, z)\, \overrightarrow{R_m^1}(kr, \varphi) + r_2(\omega_j, k, z)\, \overrightarrow{R_m^2}(kr, \varphi) \right] \right\} \tag{II-4}$$

where the sum over j is over the individual Love and Rayleigh wave modes of propagation.

Since ω only appears in the expansion weights, the expression can be integrated for a step function source time dependence as Gilbert[15] did for the free oscillation expansion to give exact expressions for a_j and b_j. These are:

$$a_j(t, k, m) = -\frac{1 - \cos \omega_j t}{(2\pi)^2\, I_L(\omega_j, k)\, \omega_j^2} \begin{bmatrix} -\frac{i\pi k}{2}\, l^*(\omega_j, k, z_s)\, (\delta_2^m - \delta_{-2}^m)\, M_{xx} \\ +\frac{i\pi k}{2}\, l^*(\omega_j, k, z_s)\, (\delta_2^m - \delta_{-2}^m)\, M_{yy} \\ -\pi k l^*(\omega_j, k, z_s)\, (\delta_2^m + \delta_{-2}^m)\, M_{xy} \\ -i\pi\, \frac{dl^*(\omega_j, k, z_s)}{dz}\, (\delta_1^m - \delta_{-1}^m)\, M_{xz} \\ -\pi\, \frac{dl^*(\omega_j, k, z_s)}{dz}\, (\delta_1^m + \delta_{-1}^m)\, M_{yz} \end{bmatrix} \tag{II-5}$$

where the normalization integral is

$$I_L(\omega_j, k) \equiv \int_o^\infty dz\, \rho(z) \left| 1(\omega_j, k, z) \right|^2$$

and

$$b_j(t, k, m) = -\frac{1 - \cos \omega_j t}{(2\pi)^2 I_R(\omega_j, k)\, \omega_j^2} \left[\begin{array}{l} \left[-\pi k \delta_0^m + \frac{\pi k}{2} (\delta_2^m + \delta_{-2}^m)\right] r_2^*(\omega_j, k, z_s)\, M_{xx} \\ + \left[-\pi k \delta_0^m - \frac{\pi k}{2} (\delta_2^m + \delta_{-2}^m)\right] r_2^*(\omega_j, k, z_s)\, M_{yy} \\ -i\pi k r_2^*(\omega_j, k, z_s) (\delta_2^m - \delta_{-2}^m)\, M_{xy} \\ + 2\pi \frac{dr_1^*(\omega_j, k, z_s)}{dz} \delta_0^m M_{zz} \\ + \pi(\delta_1^m + \delta_{-1}^m) \left[k r_1^*(\omega_j, k, z_s) + \frac{dr_2^*(\omega_j, k, z_s)}{dz} \right] M_{xz} \\ -i\pi(\delta_1^m - \delta_{-1}^m) \left[k r_1^*(\omega_j, k, z_s) + \frac{dr_2^*(\omega_j, k, z_s)}{dz} \right] M_{yz} \end{array} \right] \quad \text{(II-6)}$$

where the normalization integral is

$$I_R(\omega_j, k) \equiv \int_o^\infty dz\, \rho(z) \left[\left| r_1(\omega_j, k, z) \right|^2 + \left| r_2(\omega_j, k, z) \right|^2 \right] \quad .$$

In both Eqs. (II-5) and (II-6), δ is the Kronecker delta and z_s refers to the source depth.

To recapitulate, Eqs. (II-5) and (II-6) imply the following assumptions:

(1) The source and receiver exist in the same layered half-space,
(2) The source exists at only one point in the half-space,
(3) The source has a step function time dependence,
(4) All body wave effects are ignored, and
(5) The material is unstressed before the source acts.

With these assumptions, the six elements of the moment tensor provide a complete description of the point source. It can be decomposed uniquely into three source mechanisms: (1) symmetric or explosive source, (2) compensated linear vector dipole (CLVD) source, and (3) double couple source, provided that the principal stress directions for the latter two are coincident (Knopoff and Randall[14]). As such, the expansion is a good candidate for the application of linear estimation procedures and should provide discriminant information between explosive and earthquake sources.

D. W. McCowan

D. TEST OF THE EMPIRICAL SURFACE WAVE MAGNITUDE PATH CORRECTION

In the last SATS,[16] an empirical method of computing the path correction for surface wave magnitudes (M_S) was suggested. This method is based on the saddle-point approximation for the amplitudes of damped surface waves. One term of this approximation is inversely related to the slope of the group velocity curve, a term that had heretofore been ignored (or taken from tables for specific paths) in the computation of M_S. The crux of the proposed method is to estimate the slope of the group velocity curve directly from the individual seismogram on which the surface wave amplitudes are measured. This estimate entails measuring the period and arrival time of the surface wave phases arriving just before and after the phase on which the amplitude to be used in the M_S calculation is measured.

This method has been tested using the long-period vertical seismograms recorded at some thirty World-Wide Standard Seismograph Network (WWSSN) stations following the large underground nuclear explosion "Cannikin," detonated in the Aleutian Islands on 6 November 1971. We decided to test the method with an explosive source in order to minimize the azimuthal variation in surface wave amplitudes predicted from the double couple earthquake source. The "new" M_S formula is based on the logarithm of the amplitude of the surface wave phase, plus correction terms for geometric spreading, attenuation, and the group velocity slope estimation. The results were compared with the "old" M_S (or Prague) formula which is based on the sum of the logarithm of the ratio of the amplitude and period, and a geometric spreading term. A positive result from the experiment would be that the new method would reduce significantly the scatter (or standard deviation) of M_S measurements, at various periods and distances, over the old method.

In Fig. II-6, the old and new methods of M_S determinations, as a function of period, are compared using the Cannikin data. In this and the following comparisons, only the variable factors affecting M_S are considered; the addition of an arbitrary constant (3.3 units in the case of the old measurement) has not been made. Figure II-6 shows that, although the new M_S does not show the dependence on period seen in the old, the overall scatter in the measurements does not seem to have been significantly reduced. The trend in the old measurements can be attributed almost wholly to the use of the ratio of amplitude and period rather than amplitude alone.

Figure II-7 compares the old and new methods as a function of distance. In this diagram, it is generally the case that at a single station (distance = constant) the new measurements are less scattered than the old; however, the overall scatter is about the same. This means that the new method will give more consistent results using phases of different periods at a single station, but, again, the scatter between various phases at different stations is essentially the same.

These conclusions are quantified in the histograms of Fig. II-8 which shows the distribution of the old and new measurements. The standard deviation of the old method is 0.24 unit; that of the new is 0.22. This does not appear to be an improvement of enough significance to encourage the general use of the proposed new method of surface wave magnitude determination. Three reasons for this lack of improvement are initially suggested. An assumed attenuation correction based on a constant Q of 500 was applied in the new method. Both azimuthal and frequency dependence of Q may make this assumption invalid. Most paths from the Aleutians to any continental station are complicated by crossing ocean-continent boundaries. This may introduce errors which cannot be accounted for in the simple propagation model applied. Finally, it may be that

differences in arrival time and period, used in the estimation of the group velocity curve slope, cannot be measured accurately enough by hand.

J. R. Filson

E. RAYLEIGH-WAVE PHASE VELOCITIES ACROSS THE EURASIAN CONTINENT

Four earthquakes located within a small region of the Hindu Kush have been studied thoroughly to determine their source mechanisms (depth, slip angle, dip angle, strike, and seismic moment). Two of these earthquakes (Nos. 1 and 2) were analyzed in a previous report[16] using a surface wave method developed by Weidner and Aki.[17] This method, which is restricted to pairs of earthquakes, recently has been extended to incorporate any number of events in a cluster. Furthermore, highly refined Rayleigh-wave phase velocities for paths emanating from the source region to surrounding WWSSN stations have been obtained.

Unlike Weidner and Aki's method involving spectral ratios between an earthquake pair, the new, extended method isolates source effects on surface wave spectra for a single earthquake and then matches theoretical calculations to obtain source parameters. To accomplish this, we use earthquakes with known source mechanisms to estimate the propagational effects-amplitude attenuation, $H_j(\omega)$, and path phase delay, $\varphi_j(\omega)$, between the source region and the j^{th} station. Then, we deconvolve these effects from spectra of a new earthquake, thereby isolating its source effects. For example, if $E_{1j}(\omega)$ is the known amplitude excitation for earthquake No. 1 and $A_{1j}(\omega)$ is the observed amplitude spectrum at the j^{th} station, corrected for instrument response and geometric spreading, then

$$H_j(\omega) = \frac{A_{1j}(\omega)}{E_{1j}(\omega)} \quad .$$

Similarly, another estimate for $H_j(\omega)$ can be found using $E_{2j}(\omega)$ and $A_{2j}(\omega)$. Since these estimates are subject to errors, we make use of a statistical calculation[18] to obtain the maximum-likelihood estimate (MLE), $\hat{H}_j(\omega)$. Deconvolving this estimate from spectra of a new, third earthquake occurring in the source region

$$S_{3j}(\omega) = \frac{A_{3j}(\omega)}{\hat{H}_j(\omega)}$$

we isolate its source effects, $S_{3j}(\omega)$, which are then modeled. It should be noted that (1) an analogous procedure is carried out on the phase spectra involving the MLE for the path phase delay, $\hat{\varphi}_j(\omega)$, and that (2) as more events in the source region are solved, the estimates $\hat{H}_j(\omega)$ and $\hat{\varphi}_j(\omega)$ are steadily improved.

Using $\hat{\varphi}_j(\omega)$ obtained after four events were solved, we calculated Rayleigh-wave phase velocities for many paths between the source region and the stations shown in Fig. II-9. The dispersion for just the paths which sample the stable Russian platform are shown in Fig. II-10. The dotted lines in the first group indicate the range of dispersion observed for stable areas of the North American continent compiled by Knopoff.[19] The next group samples the Norwegian Sea as well as the platform, and thus these velocities are noticeably slower. Although the last group shows some scatter at long periods, comparison with the first group is good at periods shorter than 70 sec.

H. J. Patton

REFERENCES

1. Seismic Discrimination SATS, Lincoln Laboratory, M.I.T. (30 June 1972), DDC AD-748305; (30 June 1973), DDC AD-766559/9; and (30 June 1974), DDC AD-785377/3.
2. R. G. Rodriguez, Atlas of Eastern Europe and Asia to Support Detection of Underground Nuclear Testing, Vol. V: Crust and Mantle Conditions (Department of the Interior, U.S. Geological Survey, 1969).
3. L. Knopoff, "Structure of the Crust and Upper Mantle in the Alps from the Phase Velocity of Rayleigh Waves," Bull. Seismol. Soc. Am. 56, 1009 (1966).
4. A. M. Dziewonski, A. L. Hales, and E. R. Lapwood, "Parametrically Simple Earth Models Consistent with Geophysical Data," Phys. Earth Planet. Inter. 10, 12-48 (1975).
5. H. Bungum and J. Capon, "Coda Pattern and Multipath Propagation of Rayleigh Waves at NORSAR," Phys. Earth Planet. Inter. 9, 111-127 (1974).
6. N. A. Haskell, "Radiation Pattern of Surface Waves from Point Sources in a Multilayered Medium," Bull. Seismol. Soc. Am. 54, 377-393 (1964).
7. M. L. Gerver and D. A. Kazhdan, "Determination of Velocity Profiles from Dispersion Curves. Problems of Uniqueness," in Some Direct and Inverse Problems of Seismology, Vol. 4 of the series Computational Seismology, V. I. Keilis-Borok, Editor (Nauka Publishing House, Moscow, 1968), pp. 78-94 (in Russian).
8. N. N. Biswas and L. Knopoff, "Exact Earth Flattening Calculations for Love Waves," Bull. Seismol. Soc. Am. 60, 1123-1137 (1970).
9. B. A. Bolt and J. Dorman, "Phase and Group Velocities of Rayleigh Waves in a Spherical, Gravitating Earth," J. Geophys. Res. 66, 2965-2981 (1961).
10. F. Gilbert, personal communication.
11. D. G. Harkrider, "Surface Waves in Multilayered Elastic Media. Part II. Higher Mode Spectra and Spectral Ratios from Point Sources in Plane Layered Earth Models," Bull. Seismol. Soc. Am. 60, 1937-1987 (1970).
12. M. Saito, "Excitation of Free Oscillations and Surface Waves by a Point Source in a Vertically Heterogeneous Earth," J. Geophys. Res. 72, 3689-3699 (1967).
13. M. Foster, "An Application of the Weiner-Kolmogorov Smoothing Theory to Matrix Inversion," J. Soc. Indust. Math. 9, 387-392 (1961).
14. L. Knopoff and M. J. Randall, "The Compensated Linear Vector Dipole: A Possible Mechanism for Deep Earthquakes," J. Geophys. Res. 75, 4957-4963 (1970).
15. F. Gilbert, "Excitation of the Normal Modes of the Earth by Earthquake Sources," Geophys. J. R. Astron. Soc. 22, 223-226 (1970).
16. Seismic Discrimination SATS, Lincoln Laboratory, M.I.T. (31 December 1974), DDC AD-A006194.
17. D. Weidner and K. Aki, "Focal Depth and Mechanism of Mid-ocean Ridge Earthquakes," J. Geophys. Res. 78, 1818 (1973).
18. V. Pisarenko, "Statistical Estimates of Amplitude and Phase Corrections," Geophys. J. R. Astron. Soc. 20, 89 (1970).
19. L. Knopoff, "Observation and Inversion of Surface-Wave Dispersion," in The Upper Mantle, Tectonophys., Vol. 13, edited by A. Ritsema (Elsevier Publishing Co., Amsterdam, 1972), p. 497.

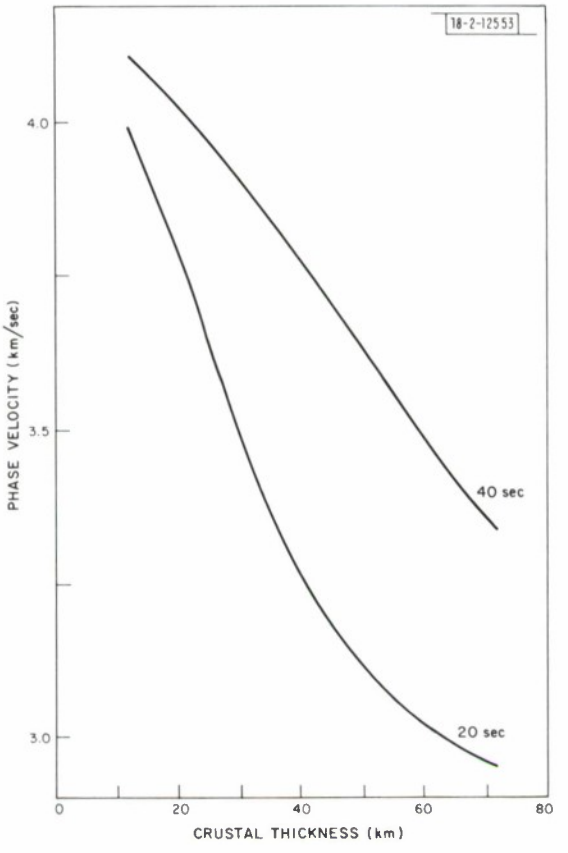

Fig. II-1. Rayleigh-wave phase velocities at 20- and 40-sec periods for crustal model used, as a function of crustal thickness.

Fig. II-2. Ray paths traced from NORSAR (60.8°N, 10.8°E) at 5° increments in azimuth from 45° to 120°. Numbers at end of each ray give final azimuthal deviation. Longest ray is to 78° distance from NORSAR.

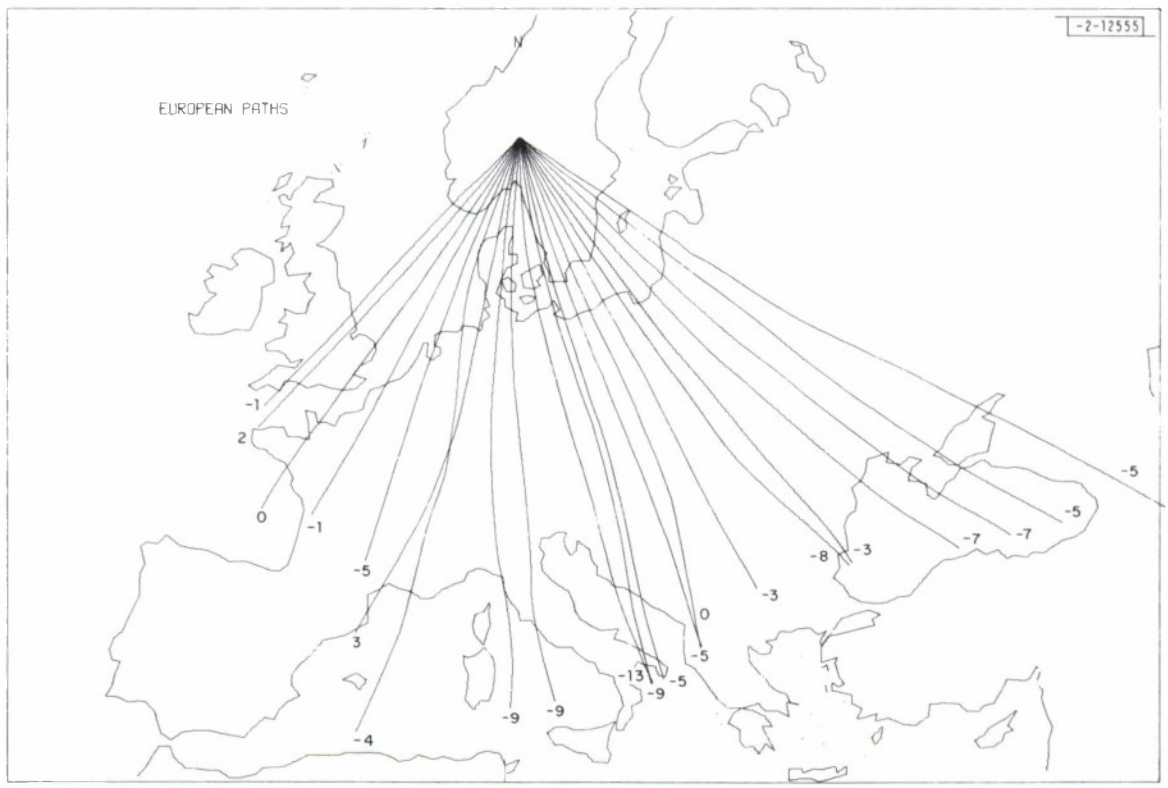

Fig. II-3. Same as Fig. II-2, but from 125° to 225° azimuth. Longest ray is to 29° distance from NORSAR.

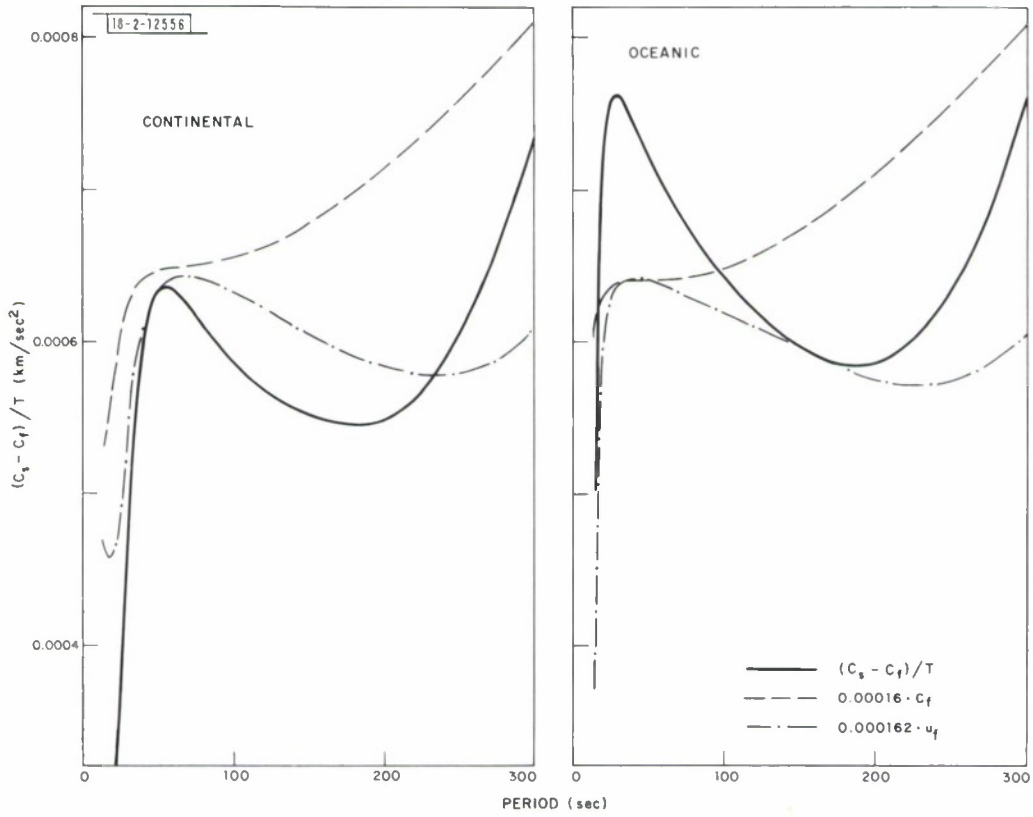

Fig. II-4. Comparison of computed values of $(C_S - C_f)/T$ with scaled phase (C_f) and group (u_f) velocity curves computed for layered half-space.

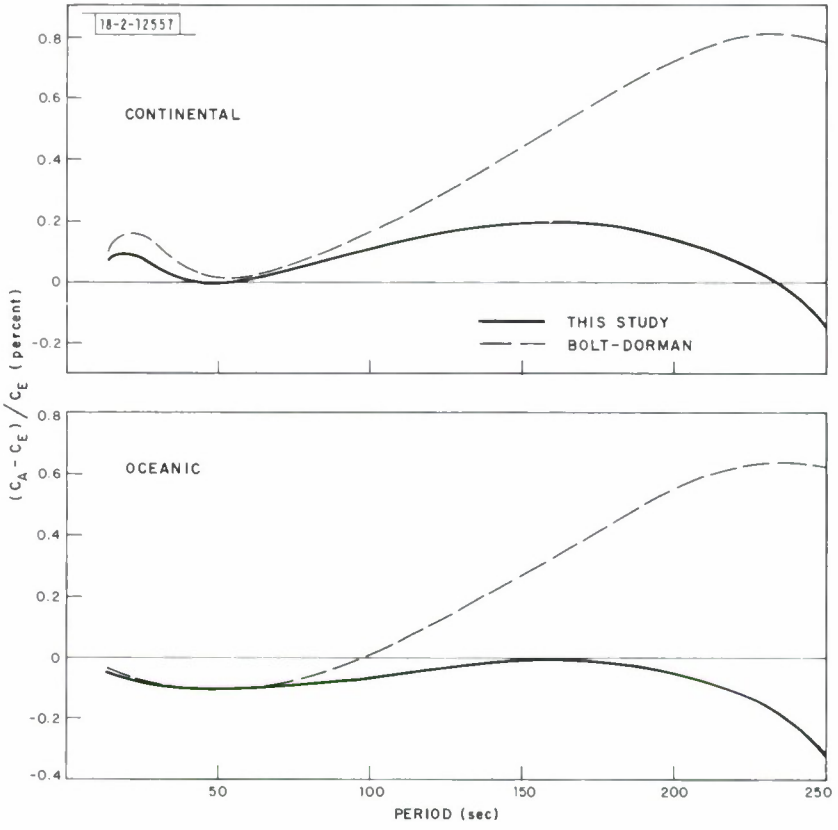

Fig. II-5. Comparison of relative errors introduced by application of empirical earth flattening correction proposed in this study (solid line) with that of Bolt and Dorman.[9] C_A designates value of phase velocity obtained using the appropriate approximate formula; C_E is the exact value.

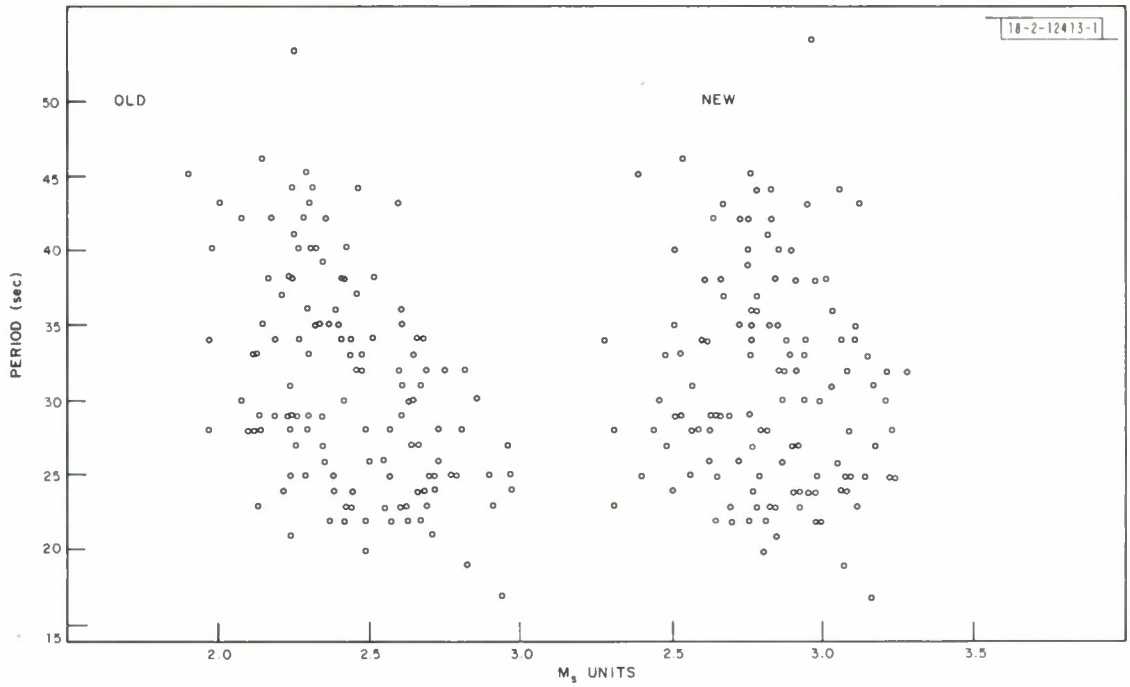

Fig. II-6. Comparison of new and old M_S measurement methods as a function of period.

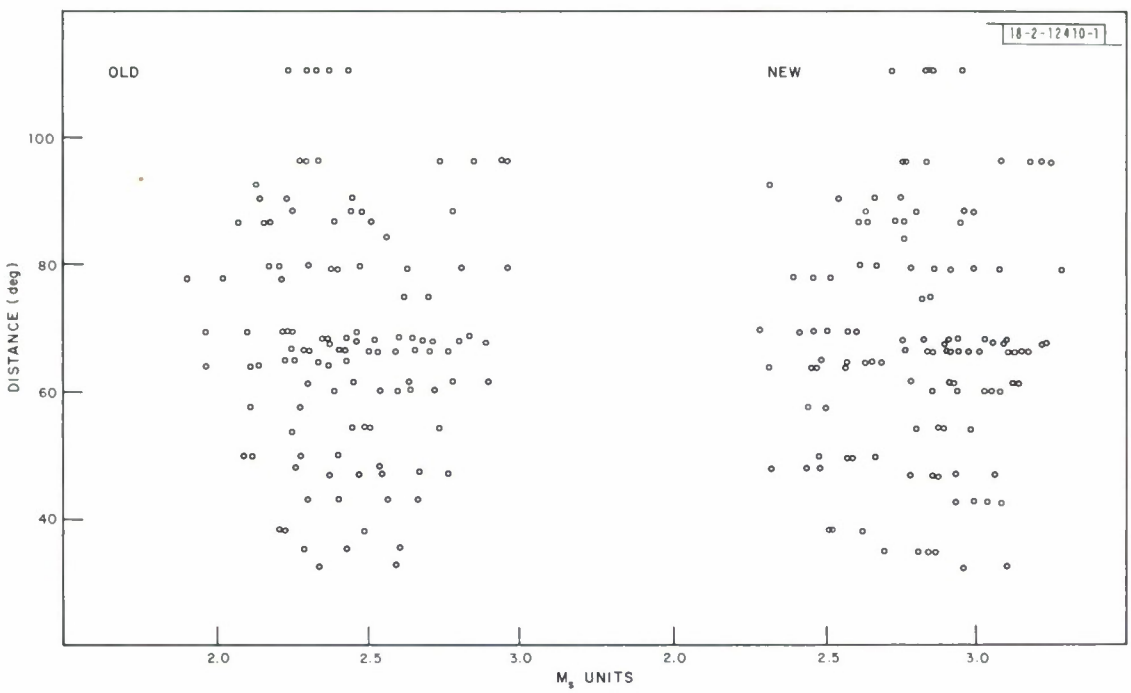

Fig. II-7. Comparison of new and old M_S measurement methods as a function of distance.

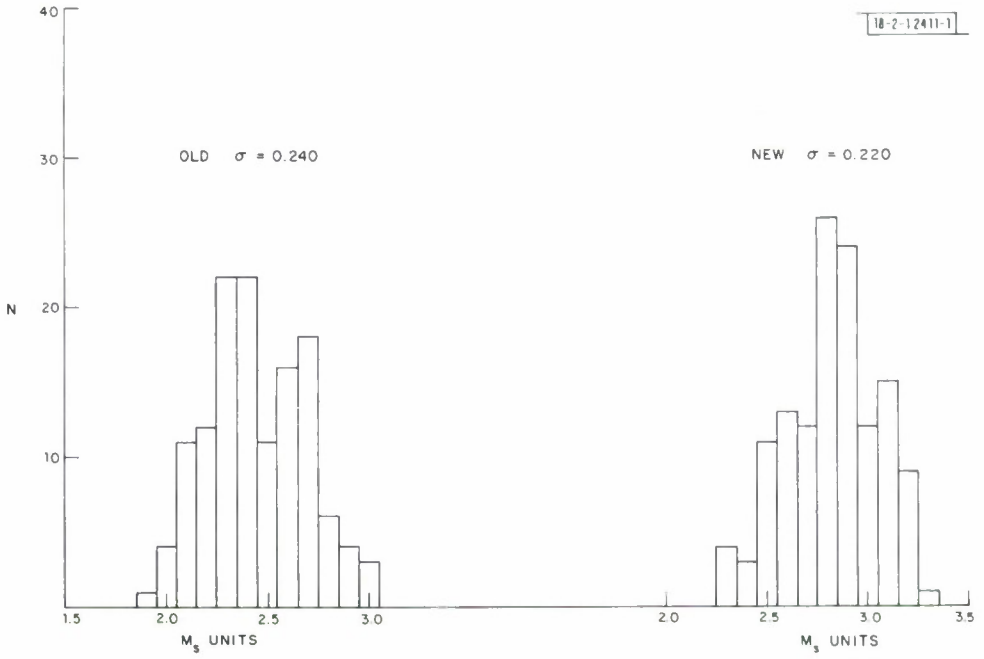

Fig. II-8. Distribution of new and old M_S measurement methods.

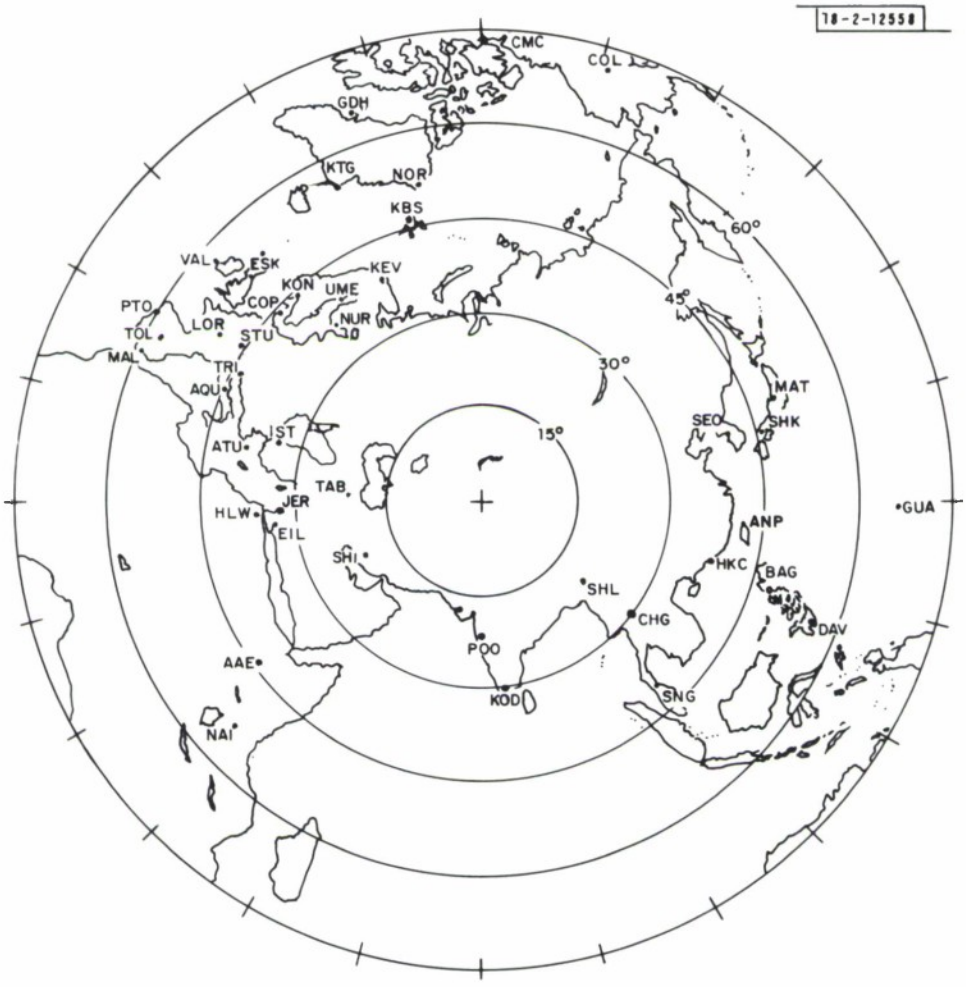

Fig. II-9. Station distribution used in this study.

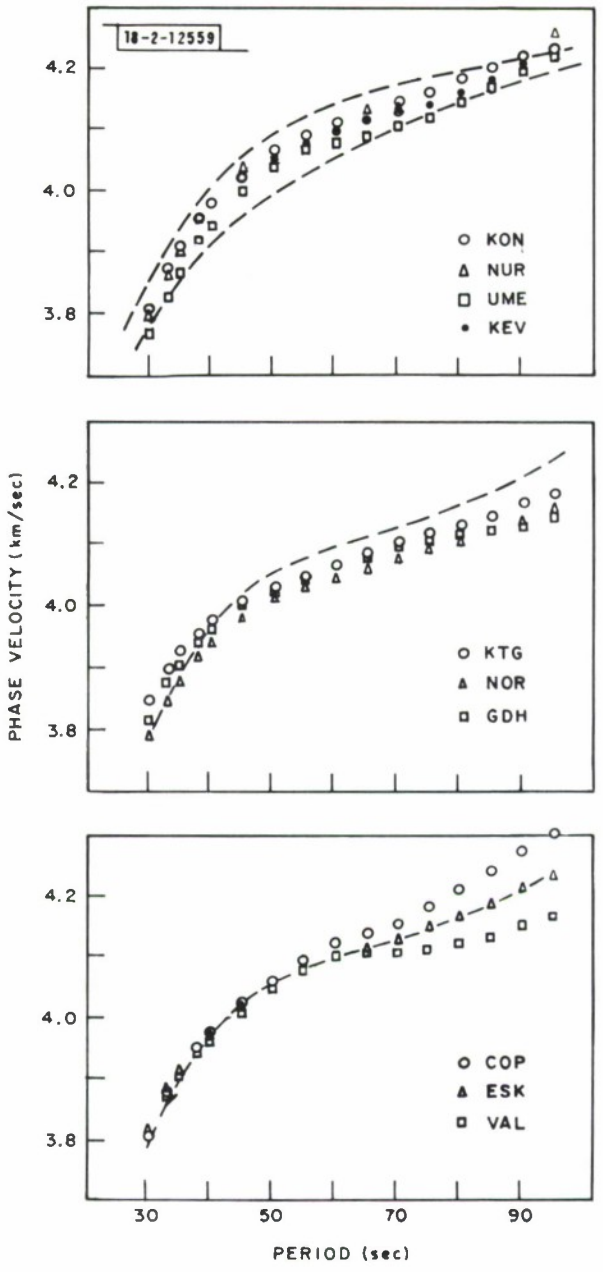

Fig. II-10. Dispersion curves for paths that sample the Russian platform.

III. EARTHQUAKE SOURCE MECHANISMS

A. P-WAVES FROM SHALLOW ASIAN EARTHQUAKES

As indicated in the last SATS,[1] a study into the usefulness of long- and short-period P-waveforms in determining source parameters and depth of shallow focus earthquakes has been undertaken. To date some seven shallow, rather large events from Asia have been studied using long-period data. The method of study consists of visually matching the long-period P-waves observed at a network of stations (here the WWSSN) to those generated by a simple model. The model seismograms are based on the sum of the phases P, pP, and sP generated by a Savage-type source,[2] this sum then being convolved with a nominal instrument response, an attenuation operator, and a geometric spreading factor. Account is made for the amplitude and phase modification of pP and sP due to reflection above the source, and for the effect of the free surface at the recording site. The effects of crustal layering near the source and receiver are ignored.

A sample of the results of this type of analysis are given in Fig. III-1 through the example of a shallow earthquake in Kashmir. Here, 13 observed seismograms (above) may be compared with the synthetic seismograms generated for that station (directly below) by the model. Both the data and the synthetic seismograms have been scaled to long-period, WWSSN, vertical seismograms at a gain of 1500. The scale gives the equivalent time and amplitude on such an instrument; the model parameters are shown beneath the diagram. A and B are the semimajor and minor axes of a plane, elliptical fault surface; RVEL is the velocity of rupture from one focus of the ellipse; C is the P-phase velocity in the source region; STRIKE is that of the fault plane measured clockwise from north; TILT is the angle the fault plane makes with the vertical; SLIP and DLOC define the direction and magnitude of a constant dislocation vector within the fault plane; and M_o gives the moment based on the product of $A \cdot B \cdot DLOC$ and a rigidity of $3 \cdot 10^{11}$ dyn/cm^2. The circle in the center of the figure represents a stereographic projection of the lower focal sphere showing the fault and auxiliary planes, and the point at which the relevant rays penetrate this hemisphere. Here, the plane on the upper right is taken to be the fault plane. In general it may be said that the model gives a fair, visual representation of the observed data, both in amplitude and phase, for the first one-and-one-half cycles. A similar example of another shallow, thrust event, this time from the Hindu Kush, is shown in Fig. III-2.

An attempt to apply the same technique to a strike-slip source is shown in Fig. III-3. This event, in northeastern Siberia, has been discussed previously. As the reader may observe, this match between the recorded and synthetic seismograms is not as good as in the case of the thrust-type sources discussed above. However, the first cycle or so, again in both phase and amplitude, is fairly well reproduced. The source parameters used to fit the long-period seismograms in Fig. III-3 were then used to generate short-period traces, and four of these are compared with the relevant observations at four stations in Fig. III-4. It would seem that this is the most important question that studies such as this address – can reliable source information be gained from short-period seismograms? A comparison of the observed and synthetic traces in Fig. III-4 shows that the short-period synthetics give a fair approximation to the general shape of the observed waveforms. Other comparisons, not shown here, are very poor. The conclusion, thus far, is that along certain paths information concerning the earthquake source is discernible in the short-period seismogram, while along other paths this information is totally masked by propagation effects.

J. R. Filson

B. EARTHQUAKE SOURCE MECHANISM DISCRIMINATION

Source mechanism discrimination for earthquakes of the mid-Atlantic ridge system has been studied and shown to be feasible. This region was studied because the mechanisms of mid-ocean ridge earthquakes are characteristically of two types: strike-slip events occurring on transform faults, and dip-slip events occurring on ridge crests.[3,4] In addition, since the earthquakes of these two mechanism types occur at similar depths,[5] the study of the two mechanism types can be approached as a two-class discrimination problem.

Parameters of the teleseismic signal other than its first motion were studied in order to identify those parameters of the signal which reflect the source mechanism differences. Among the parameters considered were surface and body wave magnitudes, P-wave signal complexity, dominant period, and spectral ratio. A set of prototype events of strike-slip (SS) or dip-slip (DS) mechanism was studied to determine which of these parameters do in fact exhibit differences for the two mechanism types. Those parameters found useful for the mechanism discrimination were M_s, m_b, and the predominant period of the P-wave (at LASA). Features, or functions having characteristically different values for events of the two classes, were then formed from these parameters, and the discrimination was based on these features.

The surface and body wave magnitudes for the events of the central mid-Atlantic ridge (from 0° to 35°N) studied here are plotted in Fig. III-5. Similarly, the P-wave predominant period for these events is plotted against surface wave magnitude in Fig. III-6. The two populations are reasonably separated in these figures, and possible lines of separation have been drawn. The features for the mechanism discrimination are based on projection of the observed data onto the normals to these separation lines. The performance of this discrimination scheme is indicated by the confusion matrix:

	SS	DS	Total
SS	24	1	25
DS	1	11	12

Thus for these data, the scheme yields one error out of 25 events in the recognition of SS events, and one error out of 12 events in the recognition of DS events. An estimate of the total probable error rate is perhaps 12 percent, or an 88-percent correct classification rate. However, this type of error estimate, based on the prototype event set, is at best a lower bound to the true probable error,[6] and must be further qualified by the relatively small sample size. However, the separation of the populations in Figs. III-5 and III-6, on which the discrimination is based, is statistically significant at the 95-percent level.

These results can be interpreted in terms of the physical environment at the ridge. The differences which might be observed in M_s and m_b, due solely to differences in the surface and body wave radiation patterns for different types of faulting, can be estimated from the formulations of Harkrider[7] and Ben-Menahem et al.[8] For the same moment and source time function, the estimated changes in M_s and m_b from their values for vertical strike-slip faulting are, for vertical dip-slip faulting and dip-slip faulting on a 45° plane:

	ΔM_s	Δm_b
Vertical DS	−0.2	+0.6
45° DS	−0.3	+0.8

In Fig. III-5, the M_s vs m_b positions of a vertical dip-slip event and a 45° dip-slip event are indicated, given that a vertical strike-slip event has an M_s vs m_b typical for the observed SS population.

The presence of a zone of high attenuation under ridge crests but not under transform faults will have an effect on the M_s-m_b values opposite to that of the source mechanisms. The source mechanism effect will tend to separate the two populations, while a zone of high attenuation under the ridge DS events will reduce their m_b, driving the DS population back into the SS population. If the clustering of the two populations in Fig. III-5 is due to greater attenuation for DS events, then that attenuation is apparently causing a reduction of the DS body magnitudes by roughly 0.5 unit more than the reduction in SS body magnitudes. If the transform events are relatively unattenuated, and the attenuating zone under the ridge crest is of the dimensions (~100 km) suggested by Solomon and Julian,[9] then the reduction in magnitude requires a Q of about 40 in this zone, consistent with the estimate by Solomon[10] of Q ~ 10 for S-waves. Also, if the clustering of the populations is due to greater attenuation for the DS events, discrimination between these two mechanism types should be easier in a region without this differential attenuation.

A. F. Shakal

REFERENCES

1. Seismic Discrimination SATS, Lincoln Laboratory, M.I.T. (31 December 1974), DDC AD-A006194.
2. J. Savage, "Radiation from a Realistic Model of Faulting," Bull. Seismol. Soc. Am. 56, 557-592 (1966).
3. L. R. Sykes, "Mechanism of Earthquakes and Nature of Faulting on the Mid-Oceanic Ridges," J. Geophys. Res. 72, 2131-2153 (1967).
4. L. R. Sykes, "Seismological Evidence for Transform Faults, Sea Floor Spreading, and Continental Drift," in The History of the Earth's Crust, R. A. Phinney, Editor (Princeton University Press, New Jersey, 1968), pp. 120-150.
5. D. J. Weidner and K. Aki, "Focal Depth and Mechanism of Mid-Ocean Ridge Earthquakes," J. Geophys. Res. 78, 1818-1831 (1973).
6. K. Fukunaga, Introduction to Statistical Pattern Recognition (Academic Press, New York, 1972).
7. D. G. Harkrider, "Surface Waves in Multilayered Elastic Media. Part II. Higher Mode Spectra and Spectral Ratios from Point Sources in Plane Layered Earth Models," Bull. Seismol. Soc. Am. 60, 1937-1987 (1970).
8. A. Ben-Menahem, S. W. Smith, and T. L. Teng, "A Procedure for Source Studies from Spectrums of Long Period Seismic Body Waves," Bull. Seismol. Soc. Am. 55, 203-235 (1965).
9. S. C. Solomon and B. R. Julian, "Seismic Constraints on Ocean-Ridge Mantle Structure: Anomalous Fault-Plane Solutions from First Motions," Geophys. J. R. Astron. Soc. 38, 265-285 (1974).
10. S. C. Solomon, "Shear-Wave Attenuation and Melting Beneath the Mid-Atlantic Ridge," J. Geophys. Res. 78, 6044-6059 (1973).

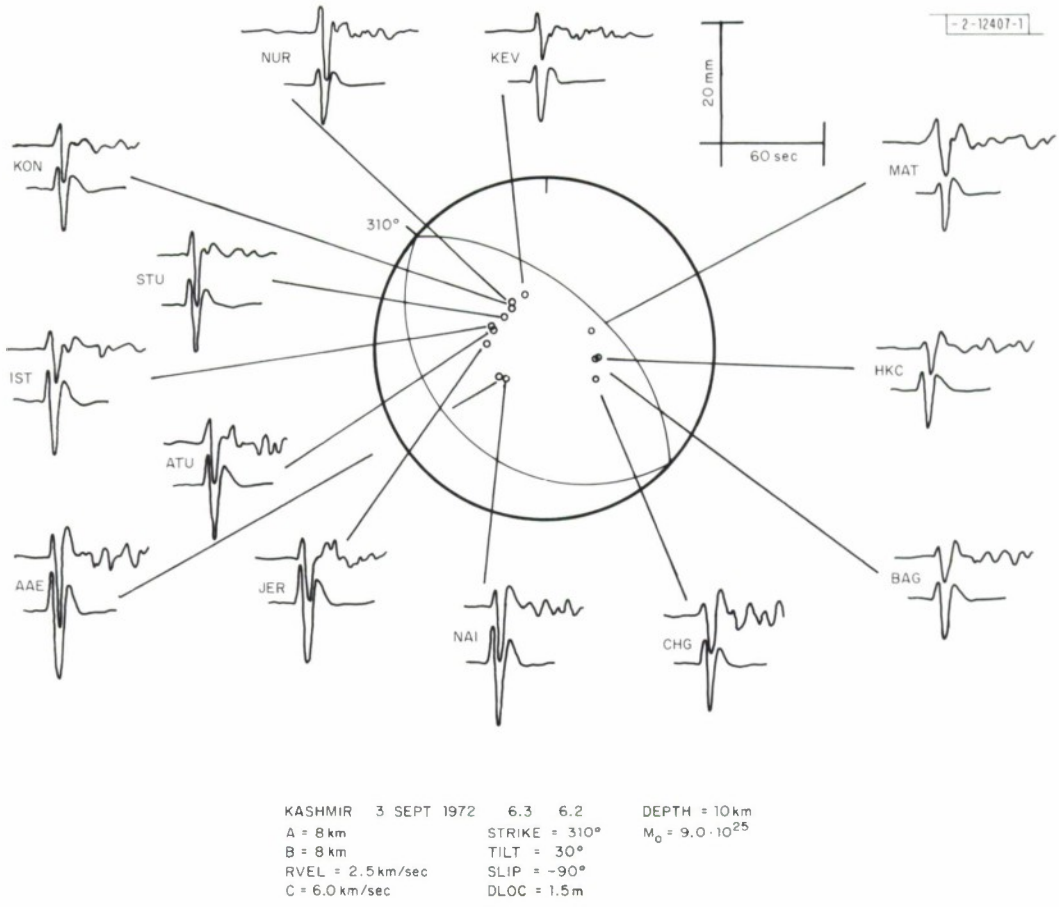

Fig. III-1. Comparison of observed (above) and synthetic (below) long-period P-wave seismograms for shallow thrust earthquake in Kashmir.

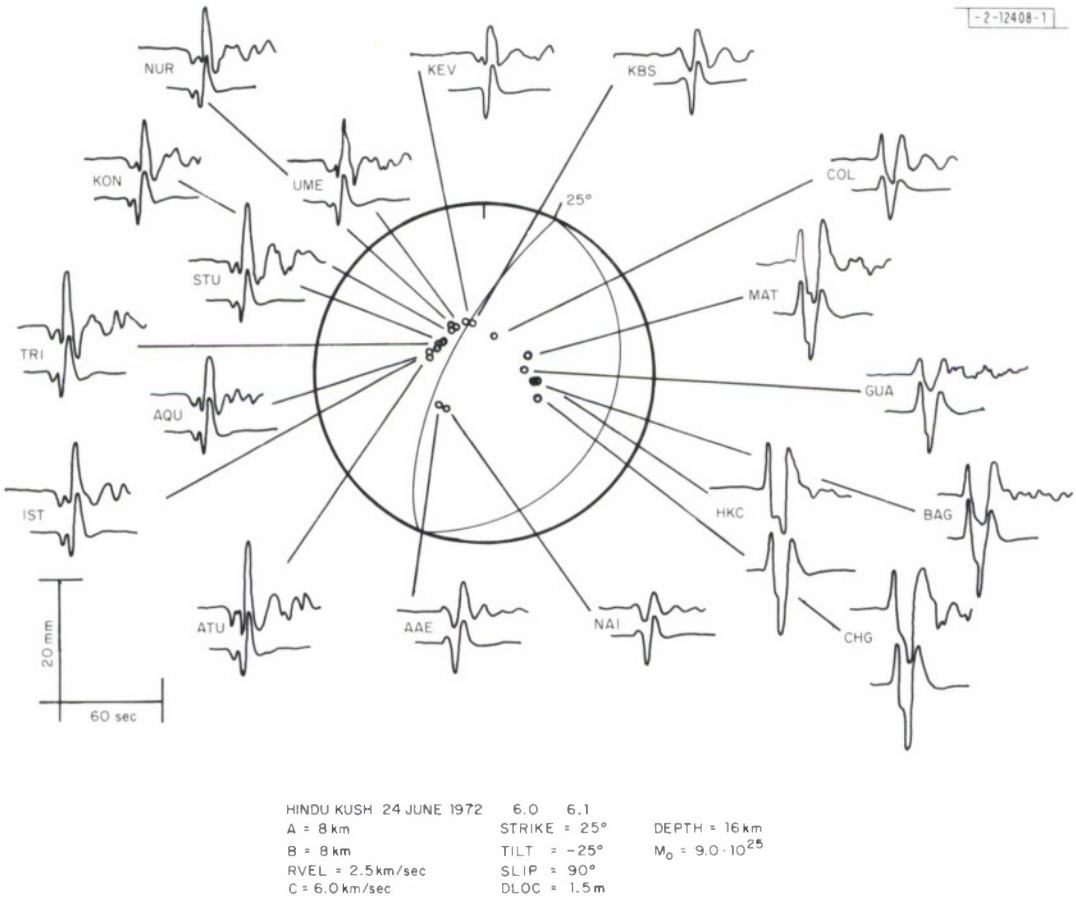

Fig. III-2. Comparison of observed (above) and synthetic (below) long-period P-wave seismograms for shallow thrust earthquake in Hindu Kush.

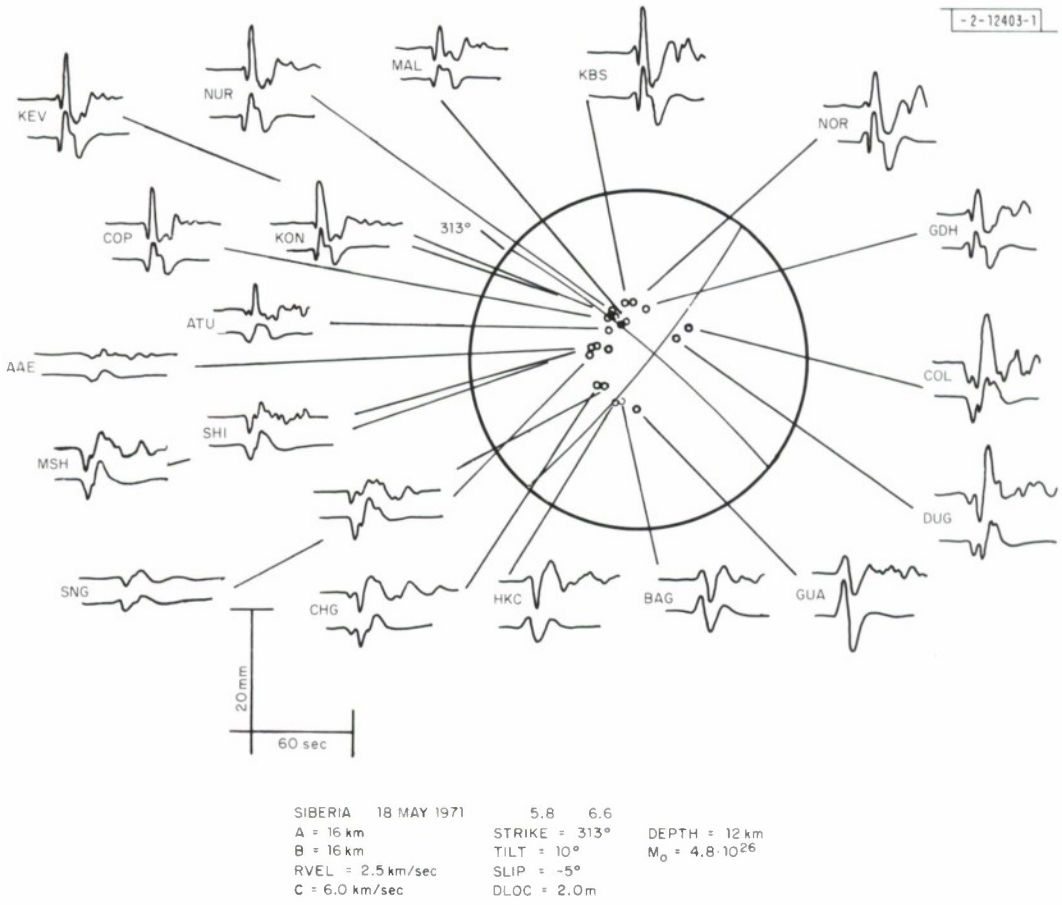

Fig. III-3. Comparison of observed (above) and synthetic (below) long-period P-wave seismograms for shallow strike-slip earthquake in Siberia.

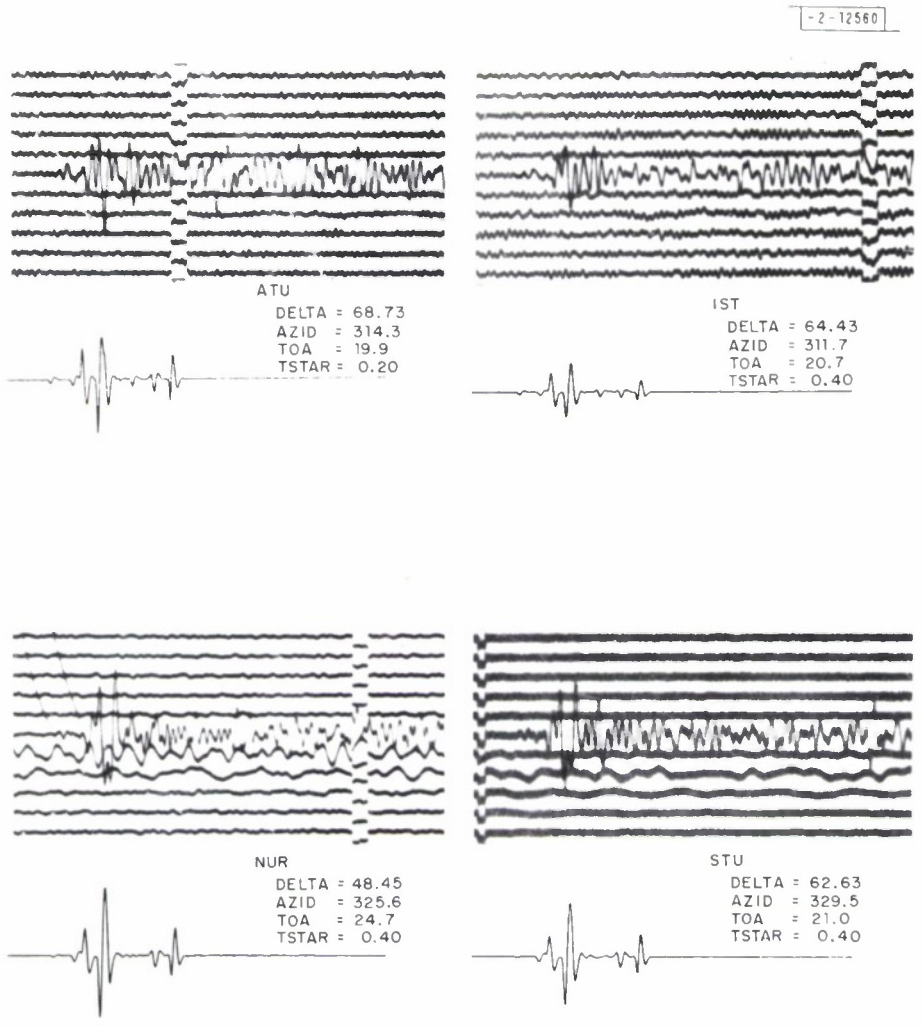

Fig. III-4. Comparison of observed and synthetic short-period seismograms at four European stations for Siberian event of Fig. III-3.

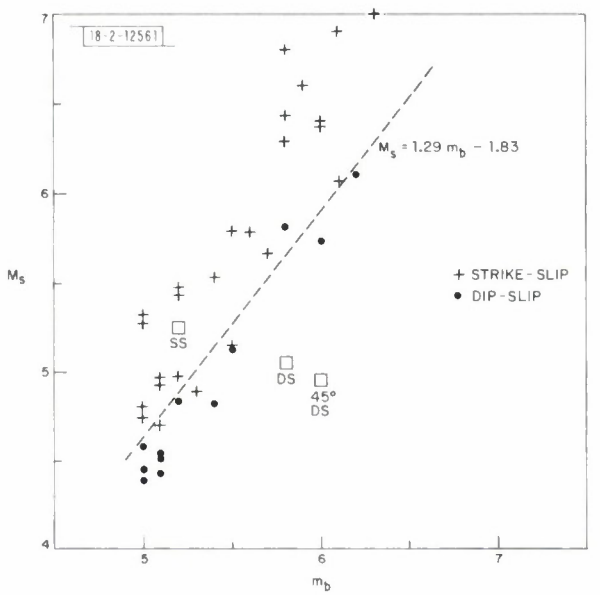

Fig. III-5. Surface and body wave magnitudes for central mid-Atlantic ridge events of this study, with possible line of separation between two event types. Also indicated are relative M_S-vs-m_b positions of 90° DS and 45° DS events, estimated in text, given that M_S vs m_b of a vertical SS event is as indicated.

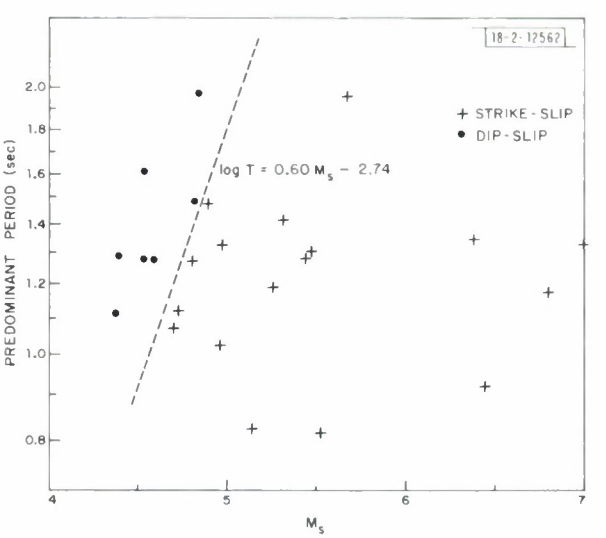

Fig. III-6. Predominant period of LASA P-wave vs M_S for events of Fig. III-5 for which LASA signal was available.

IV. EARTH HETEROGENEITY AND SCATTERING

A. SYSTEMATIC INVERSION FOR LARGE-SCALE HETEROGENEITIES IN THE MANTLE: PRELIMINARY RESULTS

Global studies of the radial velocity distribution have been limited so far to the "average" earth. This corresponds to the zero-order coefficient in the spherical harmonic expansion of the velocities in the laterally heterogeneous earth. Availability of a large number of travel time observations reported to the International Seismological Center (ISC) makes feasible an attempt at extracting the coefficients for several low-order harmonics of the lateral variations in the distribution of compressional velocity. If the experiment were successful, some fundamental geophysical questions might be answered. Also, availability of a three-dimensional velocity model could improve the accuracy of location of seismic events.

Data for P and PKIKP travel times were extracted from the ISC Bulletins for the years 1964 to 1970 for events with magnitude ≥ 4.8 or more with 50 stations reporting. Data for phases that are subject to frequent misinterpretations were rejected, particularly P for distances $<27°$ and PKIKP for $\Delta < 160°$. Also, arrival times with residuals >5 sec were discarded as gross errors. After correction for ellipticity,[1] the total number of retained observations is 728,072. Differences between the ISC travel times and the times computed for the PEM[2] represent the data set used to determine the three-dimensional perturbations in velocity.

The inverse problem is approached by the linear approximation of the perturbation of travel times by small changes in velocity distribution.[3,1] A discrete model is adopted in this study, although other representations also are feasible.

Discretization is achieved by dividing the mantle into several concentric shells, and then partitioning each shell into conical blocks of equal latitudinal and longitudinal extent. Perturbation of velocity is assumed to be constant within a block. During its travel through each concentric shell, a seismic ray may cross one or more boundaries between adjacent blocks; in this case, it is assumed that the contribution to the observed travel time residual comes from the block in which the ray spends the most time. An example of actual discretization, together with results of inversion, is shown in Table IV-1.

The matrix inversion is performed using the singular value decomposition technique. For the example shown, 119 out of 120 possible eigenvalues were statistically significant. The perturbation reduces the overall rms error by only 30 percent; thus, it is obvious that there also must exist velocity variations of a shorter wavelength. The rms variation of perturbation in each shell is small – it ranges from 0.3 percent for the upper mantle to 0.1 percent for Region III. The fact that lateral variations are the least in the middle mantle is in agreement with the results of Julian and Sengupta,[4] who used only deep events; the data in this study were dominated by shallow focus sources.

Figures IV-1(a) through (d) show lateral variations in velocity obtained by the least-squares fit of spherical harmonics up to the third degree to results in Table IV-1; the areas of individual blocks were used as weighting factors. It is interesting to notice that velocity variations in Regions III and IV are strongly correlated. The zones in the east Pacific and southern Asia are anomalous at all levels.

Several experiments have been performed to check the stability of the solution. First, results were compared using data with and without corrections for ellipticity. In the latter case, one obtains velocity perturbations strongly influenced by the zonal harmonic of degree 2 – exactly

TABLE IV-1

RESULTS OF INVERSION FOR LATERAL VARIATIONS IN COMPRESSIONAL VELOCITY. AVERAGE PERTURBATION OF VELOCITY $\Delta\overline{V}$ IS REMOVED FROM THE VALUES REPORTED FOR INDIVIDUAL BLOCKS.

Latitude	Longitude	Region I (0 to 670 km)			Region II (670 to 1400 km)			Region III (1400 to 2200 km)			Region IV (2200 to 2880 km)		
		Number of Rays	ΔV (m/sec)	Standard Error (m/sec)	Number of Roys	ΔV (m/sec)	Standard Error (m/sec)	Number of Rays	ΔV (m/sec)	Standard Error (m/sec)	Number of Rays	ΔV (m/sec)	Standard Error (m/sec)
			−26.6*			−24.6*			−12.6*			6.5*	
90°N-54°N	0°-60°E	76,541	−3	0.9	101,967	27	1.0	70,203	−18	0.7	23,671	−2	1.1
	60°E-120°E	9,186	−10	1.3	16,506	32	1.0	58,410	3	0.5	83,016	16	0.8
	120°E-180°E	24,939	26	0.8	59,653	6	0.6	97,420	4	0.5	21,411	6	1.1
	180°W-120°W	88,717	−3	0.6	114,355	−2	0.6	61,863	6	0.6	21,057	−22	1.1
	120°W-60°W	38,499	40	0.8	30,363	4	0.9	28,790	14	0.8	10,994	−22	1.4
	60°W-0°	17,880	−13	1.1	15,876	−10	1.2	21,712	−12	0.9	14,925	−2	1.4
54°N-18°N	0°-60°E	159,817	−58	1.0	133,952	44	1.2	43,338	11	0.8	7,610	−14	1.9
	60°E-120°E	100,814	−45	0.9	105,547	38	0.9	97,457	5	0.4	58,890	21	0.6
	120°E-180°E	228,414	10	0.7	188,505	1	0.7	77,533	−6	0.5	44,138	21	0.7
	180°W-120°W	71,394	10	0.9	94,153	−38	0.9	83,586	−20	0.6	49,957	10	0.8
	120°W-60°W	161,362	13	0.7	141,052	−20	1.0	60,363	23	0.6	19,808	25	1.1
	60°W-0°	22,371	−26	1.2	28,485	13	1.2	29,307	−4	0.9	19,889	−1	1.1
18°N-18°S	0°-60°E	16,718	−32	2.0	16,575	30	1.9	13,023	−10	1.4	3,523	−13	2.5
	60°E-120°E	37,948	−49	1.2	44,698	51	1.1	32,395	−2	0.9	13,988	13	1.1
	120°E-180°E	144,306	−23	1.0	133,638	31	1.1	73,274	4	0.6	23,885	−10	1.0
	180°W-120°W	18,069	17	1.6	22,734	35	1.7	28,933	14	1.5	51,614	25	1.0
	120°W-60°W	67,038	0	1.0	55,606	−1	1.1	40,281	−25	0.8	17,572	−37	1.5
	60°W-0°	14,714	20	1.8	12,041	−1	1.8	8,538	−5	1.6	9,357	10	1.5
18°S-54°S	0°-60°E	8,683	2	2.9	7,810	32	3.1	5,777	−14	2.6	992	−67	4.3
	60°E-120°E	5,734	−5	2.1	3,304	31	2.9	3,772	−12	2.1	4,150	−35	2.4
	120°E-180°E	57,018	−53	1.5	63,743	41	1.6	22,884	8	1.1	7,306	−10	2.5
	180°W-120°W	31,917	25	1.5	18,822	−42	2.0	9,191	−14	2.4	2,997	−9	3.3
	120°W-60°W	26,376	47	1.6	19,039	−23	1.8	6,670	−12	2.3	3,501	0	2.9
	60°W-0°	1,554	36	3.9	4,983	−36	3.0	5,168	0	2.0	4,980	−22	2.3
54°S-90°S	0°-60°E	1,887	17	4.7	2,227	16	5.0	1,106	−4	5.6	596	20	6.3
	60°E-120°E	5,159	6	4.2	4,488	2	4.8	2,337	4	3.8	1,319	21	4.1
	120°E-180°E	6,661	−13	3.4	6,376	−27	3.4	5,292	7	2.0	4,792	0	3.0
	180°W-120°W	4,017	14	4.8	3,975	−63	5.2	3,245	30	3.1	1,269	51	4.8
	120°W-60°W	2,119	19	4.2	2,089	−39	4.1	1,944	−12	3.7	1,009	17	4.8
	60°W-0°	6,292	33	4.4	3,582	−62	5.3	2,080	40	2.7	674	5	6.1
Total number of block samplings and rms		1,456,144	27.5		1,456,144	31.9		995,892	14.7		528,890	22.9	

*Average

as expected. To check whether the large differences in the number of rays sampling individual blocks may introduce a bias, the data were counterweighted according to the number of connections between the blocks containing the source and the receiver. The resulting change in the pattern of velocity anomalies was insignificant. An allowance also was made for the possibility that the radius of the 670-km discontinuity may be variable. In this case, the change in radius represented an additional 30 parameters. The number of significant eigenvalues was 132 out of 150 possible. This indicates that the resolution for this parameter is relatively poor; however, only results for Region II, immediately underlaying the discontinuity, were appreciably changed. Perturbations in the radius occasionally reach 40 km; these are rather large, but differences of tens of kilometers have been reported on the basis of observations of P'P' reflections.[5]

Finally, Hager[6] took the results for the case with a variable radius of the 670-km discontinuity, assumed that density perturbations are proportional to velocity variations according to Birch's law,[7] computed equivalent geoid heights, and compared them with the observed heights.[8] He has found that there are statistically significant (at the 98-percent level) correlations between the observed geoid heights (with respect to the hydrostatic spheroid of reference) and separate contributions from the upper and lower mantles. These contributions are of opposite sign, such that approximately 80 percent of the effect is canceled by addition. The sum of the contributions does not show significant correlation with observations because of the noise in the velocity structure, but it has the correct magnitude.

These results, if confirmed by further tests, could be of fundamental importance. Gravitational compensation between the upper and lower mantles indicates transport of the material between these two regions. Good correlation with the gravity anomalies, calculated with respect to the hydrostatic ellipsoid rather than the ellipsoid of observed flattening, indicates that the "equatorial bulge" is an expression of a lateral heterogeneity rather than a residuum of the earth's flattening when it rotated with higher angular velocity. The latter interpretation has led to estimates of the lower-mantle viscosity as high as 6×10^{26} stokes and was used as a strong argument against convection in the lower mantle.[9]

Even though the results presented here are encouraging, it is necessary to perform further experiments before firm conclusions may be drawn. In particular, tests are needed to investigate the stability of the solution with respect to major changes in the discretization system.

A. M. Dziewonski

B. DETERMINATION OF THE THREE-DIMENSIONAL STRUCTURE OF THE LITHOSPHERE

A new approach to three-dimensional seismic modeling of the lithosphere has been studied. In contrast to conventional methods, the assumption of uniform material property within a layer is relaxed, making it possible to accommodate more complex geological structures. Another important feature is that we can estimate a lower limit of the true rms velocity perturbations in the lithosphere, under the assumption of ray-theory. Using NORSAR P-wave residuals for teleseismic events, we have estimated the three-dimensional seismic anomalies in the lithosphere to the depth of 126 km beneath the array. The fit to the observations is excellent, as indicated in the final residual comparable to the measurement error. We found clear evidence of pipe-like structures below Moho, dipping northward and away from the surface contours of the Oslo Graben (see Fig. IV-2). These pipe-like structures were interpreted as vestiges of magma ascent due to penetrative convections associated with the Permian volcanism of

Oslo Graben. The northward inclination of the pipe-like structures is interpreted as a result of plastic deformation of the lithosphere due to the shear exerted by the asthenosphere convection current driving the plate motion.

Our results also show that the velocity fluctuations are of the same order in the crust as in the upper mantle, at least to the depth of 126 km. The rms of the true velocity fluctuations in the crust and upper mantle under NORSAR is at least 3.4 percent, and is in agreement with estimates obtained from a statistical analysis of P-time fluctuation based on the Chernov theory.

K. Aki
L. A. Christoffersson
E. Husebye

C. THREE-COMPONENT ANALYSIS OF SEISMIC CODAS FROM NOVAYA ZEMLYA EXPLOSIONS

Six presumed nuclear explosions from Novaya Zemlya were studied using three-component, short-period data from the D2 subarray at LASA. The results show that each coda contains a large number of strong, impulsive body phases scattered by inhomogeneities in and out of the diametral plane. In particular, strong phases on the SH and SV components arrive several seconds after the P-arrival, and continue to arrive for at least 4 minutes of coda for each event.

Two northern events, with body wave magnitudes 6.7 and 6.8, have remarkably similar codas, suggesting identical site locations for the two events. The remaining two northern events, with magnitudes 6.1 and 6.3, have codas which match each other reasonably well, but do not match the codas of the first two events. To the south, the two events have magnitudes 6.0 and 6.9, the codas which do not clearly match each other or any of the codas of the northern events. This indicates that small changes in source location or site characteristics may completely alter the complexity of the coda arriving at distant stations.

Table IV-2 is a list of the six events, and Fig. IV-3 shows their PDE locations as black dots. Four of the events are clustered at approximately 73°N 55°E, and the remaining two are located further south near 71°N 54°E. The three-component data were rotated to radial horizontal (R), vertical (Z), and tangential horizontal (T) directions, and filtered to enhance polarized body waves.[10]

TABLE IV-2

LIST OF PRESUMED NUCLEAR EXPLOSIONS AT NOVAYA ZEMLYA

Event	Date	Origin Time (GMT)	Latitude (°N)	Longitude (°E)
1	14 Oct 1969	7:00:06	73.40	54.81
2	28 Aug 1972	5:59:57	73.34	55.09
3	14 Oct 1970	5:59:57	73.32	55.15
4	12 Sep 1973	6:57:43	73.30	55.16
5	27 Sep 1973	6:59:58	70.76	53.87
6	27 Oct 1973	6:59:57	70.78	54.18

Figure IV-4 shows the three components of Event 1 before and after the polarization filtering. A striking feature of the unfiltered data is the high levels of coda energy on the R and T components minutes after the P-wave. The filtered components show a succession of impulsive events arriving throughout the coda. These events are highly polarized P- and S-body phases of all azimuths and dips. The suppressed portions of the coda cannot be dominantly P-energy radiated from the source region but must be overlapping arrivals of scattered P- and S-waves from different regions as well as locally generated surface waves, which produce particle motions which are not clearly polarized. This suggests that scattering regions are more numerous and complex than usually deduced from array studies of Z-components only.[11]

Figures IV-5, IV-6, and IV-7 display the polarized components Z, R, and T of all six events, each scaled to $m_b = 6.5$. In Fig. IV-5, the Z-components of Events 3 and 4 with $m_b = 6.7$ and 6.8, respectively, are nearly identical for the duration of the coda displayed. This suggests that the two events have close or identical site locations, as indicated by the PDE locations in Fig. IV-3. The Z-components of Events 1 and 2, with magnitudes 6.1 and 6.3, respectively, also match but not as well as Events 3 and 4.

The four events were relocated using a common set of nineteen WWSSN stations. The revised locations are shown by circles in Fig. IV-3. It appears that the events group themselves into two pairs which are separated by 10 km. Although the absolute locations may be questionable, the separation between pairs is probably real. The difference in arrival times between the pairs is on the average about 3- to 10-times larger than the variation in station residuals at the stations most sensitive to the geographic separation.

The mismatch in polarized codas between the two pairs of events suggests that 10 km is a large enough separation to cause the codas to be uncorrelated. Correlation coefficients between similar components of Events 3 and 4 are very high, typically >0.8 for 4 minutes of data using windows 50 sec long. Events 1 and 3, however, have essentially uncorrelated components with correlation coefficients between −0.3 to +0.3.

Events 5 and 6, located at the southern end of Novaya Zemlya, are separated by 10 km according to the PDE locations. Using a set of 20 stations, they were both relocated about 10 km to the west with no change in separation. Figure IV-5 shows that the polarized codas of these two events do not match each other or the codas of the northern events. This suggests that Events 5 and 6 are separated by more than the correlation distance for scattered waves produced by the heterogeneities near Novaya Zemlya.

Beams of Events 1 to 4 are displayed in Figs. IV-5, IV-6, and IV-7. Some of the phases shown on the beams are very coherent for all four events. These phases represent strong scatterers in the mantle, and are being studied in detail.

C. W. Frasier
M. Yang
R. E. Needham

D. SCATTERING OF ELASTIC WAVES FROM DEPTH-DEPENDENT INHOMOGENEITIES

A new approximate solution has been developed for calculating the reflection and transmission coefficients for plane elastic waves incident to a transition zone in which elastic parameters vary with depth. The method is approximate in that primary scattering with no multiples is calculated at each depth point of the transition zone. The effect of the total transition zone is obtained by integrating the primary scattered field over the total depth thickness of the zone. Surprisingly,

the method seems to be accurate for transition zones in which elastic parameters vary smoothly except at frequencies near 0 Hz.

Briefly, the method associates with each element ΔZ in the transition zone a scattered wave which may contribute to either a reflection or transmission response. For the reflection response rpp, for example, the scattered amplitude from an element ΔZ is given by Bortfeld[12] as

$$\Delta rpp = \left\{ \left[\cos(2j) - \frac{1}{2} \right] \frac{\rho'}{\rho} + \frac{1}{2 \cos^2 i} \frac{\alpha'}{\alpha} - 4 \sin^2 j \frac{\beta'}{\beta} \right\} \Delta Z \qquad \text{(IV-1)}$$

where i and j are incident P- and SV-wave angles, respectively, at depth Z, and primes (') indicate derivatives of parameters with respect to Z. The phase factor associated with this scattered amplitude is given by

$$\exp[-i\omega(sx + 2\tau_\alpha)] \qquad \text{(IV-2)}$$

where s is the horizontal slowness of the wave in the x-direction, and τ_α is the one-way vertical delay time from the top of the transition zone to the scattering element ΔZ. The total reflected primary response is obtained by integrating the product of Eqs. (IV-1) and (IV-2) over the transition zone thickness. Thus,

$$RPP(\omega) = \int_{Z_o}^{Z_1} \frac{d}{dZ} (rpp) \exp[-i\omega(sx + 2\tau_\alpha)] \, dZ \quad . \qquad \text{(IV-3)}$$

By a change of integration variable from depth Z to arrival time $t = sx + 2\tau_\alpha$, Eq. (IV-3) can be written as

$$RPP(\omega) = \int_{-\infty}^{+\infty} \frac{d}{dZ} (rpp) \frac{\alpha}{2 \cos i} e^{-i\omega t} \, dt \quad . \qquad \text{(IV-4)}$$

This equation can be inverted directly to time by inspection, yielding

$$PPP(t) = \frac{d}{dZ} (rpp) \frac{\alpha}{2 \cos i} \Bigg|_{Z=Z(t)} \qquad \text{(IV-5)}$$

where Z can be calculated as a parametric function of t by evaluating the expression

$$t - sx = 2 \int_{Z_o}^{Z} \frac{\cos i \, (Z)}{\alpha(Z)} \, dZ \quad . \qquad \text{(IV-6)}$$

Similar formulas can be found for the other primary scattered responses RPS(t), RSS(t), RSP(t), TPS(t), and TSP(t). It can be shown that the responses TPP(t) and TSS(t) contain no primary interactions, so that they are approximated by weighted delta functions.

To illustrate this method, we computed reflection and transmission responses for three transition-zone models which are tabulated in Table IV-3. In Model 1, the density varies linearly with depth; Model 2 contains shear and compressional velocity gradients; and Model 3 has gradients in density and each velocity. In each model, the transition zone is 5 km thick between two elastic half-spaces.

Figures IV-8, IV-9, and IV-10 show the primary pulse shapes for Models 1, 2, and 3, respectively. Also displayed in these figures are the total reflection and transmission response shapes calculated by Haskell's layer matrix method.[13] From Fig. IV-8, it is clear that the

TABLE IV-3

PARAMETERS OF UPPER AND LOWER HALF-SPACES FOR EACH MODEL

		Model 1	Model 2	Model 3
Upper half-space	ρ_0	2.0	3.0	2.0
	α_0	5.0	5.0	5.0
	β_0	3.0	3.0	3.0
Transition zone 5 km thick				
Lower half-space	ρ_1	3.5	3.0	3.5
	α_1	5.0	8.0	8.0
	β_1	3.0	4.8	4.8

primary scattered field for Model 1, containing only a density gradient, is a very good approximation to the total scattered field. Figures IV-9 and IV-10 show some discrepancy between primary and total pulse shapes, the largest mismatches being for Model 3 in Fig. IV-10. The critical incident P-wave angle for Models 2 and 3 is 38.7°.

In order to investigate the higher-order scattering neglected in the primary pulse calculations, we computed the responses for Model 3 using a discrete time method.[14] This method, like Haskell's technique, requires a set of thin homogeneous layers to approximate a transition zone. By adjusting the layer thicknesses, the primary arrivals were constrained to arrive at equal time intervals as shown by the tall spikes in Figs. IV-11, IV-12, and IV-13. Between the large spikes are higher-order scattered arrivals which, although low in amplitude, can be dense in time. The result of this is that the total field, obtained by convolving the discrete time responses with a smoothing kernel, may look different from the primary pulse shape. This is most evident for the reflection responses at non-normal incidence, e.g., RSP and RSS.

Figures IV-14 and IV-15 show the amplitude responses for Model 3 from 0 to 2.5 Hz, calculated by three methods – two of which are the Haskell layer matrix method and the primary pulse method of this report. These responses are Fourier transforms of the pulse shapes displayed in Fig. IV-10.

Also given is the $0(1/\omega)$ response, equal to the spectrum of the initial and final discontinuities of the primary pulse shapes shown in Fig. IV-10. Except for RSS at non-normal incidence, the spectrum of the discontinuities comprises the major component of the total scattered spectrum.

For most short-period instruments, the ground velocity response rapidly falls off at 0.5 Hz and below. This implies that the primary pulse method described in this report is a quick and accurate way to compute reflection and transmission responses for sharp transition zones in the earth recorded on conventional instruments.

C. W. Frasier
P. Richards†

† Lamont-Doherty Geological Observatory, Palisades, New York 10964.

E. GLOBAL SCATTERING PARAMETERS IN THE SHORT-PERIOD BAND

Previous work[15,10] has demonstrated that the short-period codas of both local and teleseismic events observed at LASA contain considerable energy attributable to scattering by localized inhomogeneities. In order to formulate an improved model for scattering, it is necessary to determine the limits of validity of currently used models; specifically, the application of Chernov's work on acoustic waves in random liquid media to the study of seismic scattering must be examined. To do this, a program has been undertaken to determine average values for the earth of the scattering parameters used in Chernov's work.

Aki[16] has shown that for waves with frequencies greater than 1 Hz, Chernov's work breaks down when applied to LASA; so, in this study, work is being restricted to P-waves with periods of 0.25 to 1 sec. Data from LASA, NORSAR, and Russian stations will be used. The configuration of LASA and NORSAR allows the study of various scales of inhomogeneities. The very fine structure is examined by using seismometers in the A and B rings with a mean spacing of 15 km. Coarser structure is examined by using subarray sums from the A, C, D, E, and F rings with an effective mean spacing of 50 km.

The first 15 events studied cover the region along a rough arc from Alaska through the Aleutians, Kamchatka, Japan, the Philippines, Borneo, Sumatra, and the Banda Sea to the west to the Red Sea. These events will be used for the initial determination of the mean residuals near the receivers, and can be used for the study of shallow inhomogeneities near the receivers.

The next 15 events were selected from the Kurile Islands and Japan region. One-half of these events are shallow (<60 km deep), and the other half are deep (>150 km). The events were chosen along a great circle to LASA and perpendicular to the great circle to NORSAR. All the events are from 65° to 90° from LASA, to avoid the core shadow, and about 80° from NORSAR. These events are at least magnitude 5.5 and exhibit a clean impulsive P-arrival. They will be processed using methods developed in concert with Dr. A. V. Nikolaev of the Institute of Physics of the Earth and will be used to study variations in the amplitude, travel-time, and waveform of the P-arrival. These events will yield information on inhomogeneities which lie in the source region.

The final step in the study will be to attempt to study lower-mantle inhomogeneities. For this purpose, 15 events will be selected along a line from Japan to the southwest toward Taiwan and the Philippines. Rays from earthquakes with magnitude >6.5 diffracted in the D' or D" layers should give information as to whether the degree of inhomogeneity changes between these two layers. The rate at which the amplitude of PkP falls off after 90° can be used to determine whether the region near to the core-mantle boundary is more strongly inhomogeneous than the rest of the mantle.

J. Scheimer

REFERENCES

1. A. M. Dziewonski and F. Gilbert, "The Effect of Small, Aspherical Perturbations on Travel Times and a Reexamination of the Corrections for Ellipticity," Geophys. J. R. Astron. Soc. (in press, 1975).
2. A. M. Dziewonski, A. L. Hales, and E. R. Lapwood, "Parametrically Simple Earth Models Consistent with Geophysical Data," Phys. Earth Planet. Interiors 10, 12-48 (1975).
3. B. R. Julian and D. L. Anderson, "Travel Times, Apparent Velocities and Amplitudes of Body Waves," Bull. Seismol. Soc. Am. 58, 339-366 (1968).
4. B. R. Julian and M. Sengupta, "Seismic Travel Time Evidence for Lateral Inhomogeneity in the Deep Mantle," Nature 242, 443-447 (1973).
5. J. H. Whitcomb, "A Study of the Velocity Structure of the Earth by the Use of Core Phases, Part I; The 1971 San Fernando Earthquake Series Focal Mechanisms and Techtonics, Part II," Ph. D. Thesis, California Institute of Technology (1973).
6. B. Hager, "Correlation of Seismic Heterogeneities in the Mantle with Observed Gravity Anomalies," term paper for Geology 290, Harvard University (1975).
7. F. Birch, "Composition of the Earth's Mantle," Geophys. J. R. Astron. Soc. 4, 295-311 (1961).
8. W. M. Kaula, An Introduction to Planetary Physics (Wiley, New York, 1968).
9. D. P. McKenzie, "The Viscosity of the Lower Mantle," J. Geophys. Res. 71, 3995-4010 (1966).
10. Seismic Discrimination SATS, Lincoln Laboratory, M.I.T. (31 December 1974), DDC AD-A006194/5.
11. J. R. Cleary, D. W. King, and R. A. W. Haddon, "P-Wave Scattering in the Earth's Crust and Upper Mantle," Geophys. J. R. Astron. Soc. (in press, 1975).
12. R. Bortfeld, "Approximations to the Reflection and Transmission Coefficients of Plane Longitudinal and Transverse Waves," Geophys. Prosp. 9, 485-502 (1961).
13. N. A. Haskell, "The Dispersion of Surface Waves on Multilayered Media," Bull. Seismol. Soc. Am. 43, 17-34 (1953).
14. C. W. Frasier, "Discrete Time Solution of Plane P-SV Waves in a Plane Layered Medium," Geophysics 35, 197-219 (1970).
15. Seismic Discrimination SATS, Lincoln Laboratory, M.I.T. (30 June 1974), DDC AD-785377/3.
16. K. Aki and V. Chouet, "Origin of Coda Waves; Source, Attenuation, and Scattering Effects" (in press, 1975).

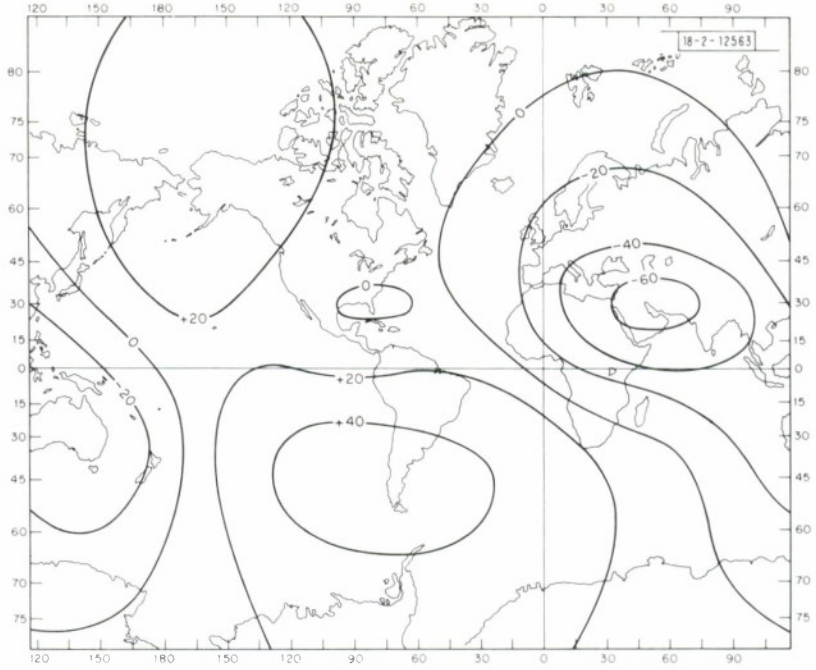

(a) Region I

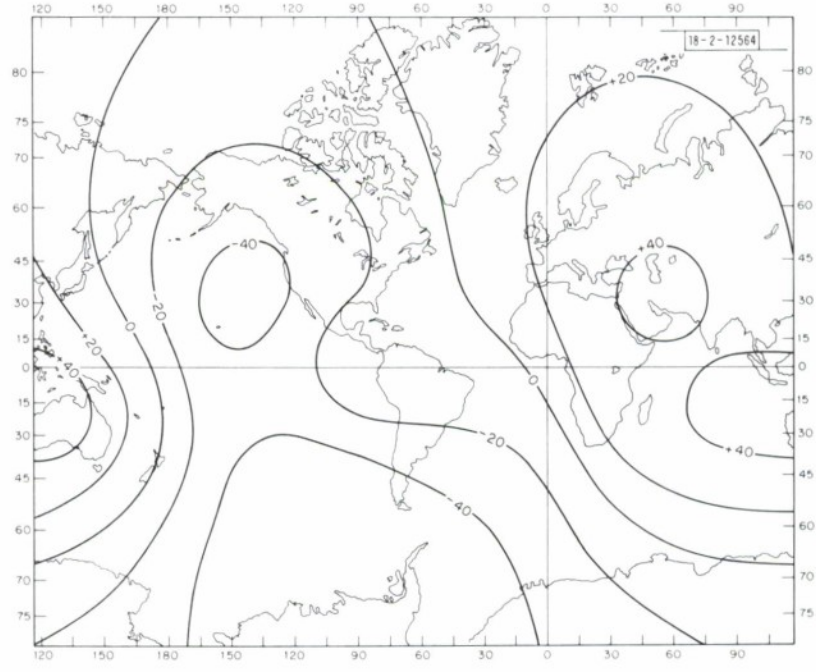

(b) Region II

Fig. IV-1(a-d). Lateral variations of compressional velocities in four concentric shells; contour units are in meters/second. Depth range of individual regions is: Region I, from 0 to 670 km; Region II, from 670 to 1400 km; Region III, from 1400 to 2200 km; and Region IV, from 2200 km to core-mantle boundary.

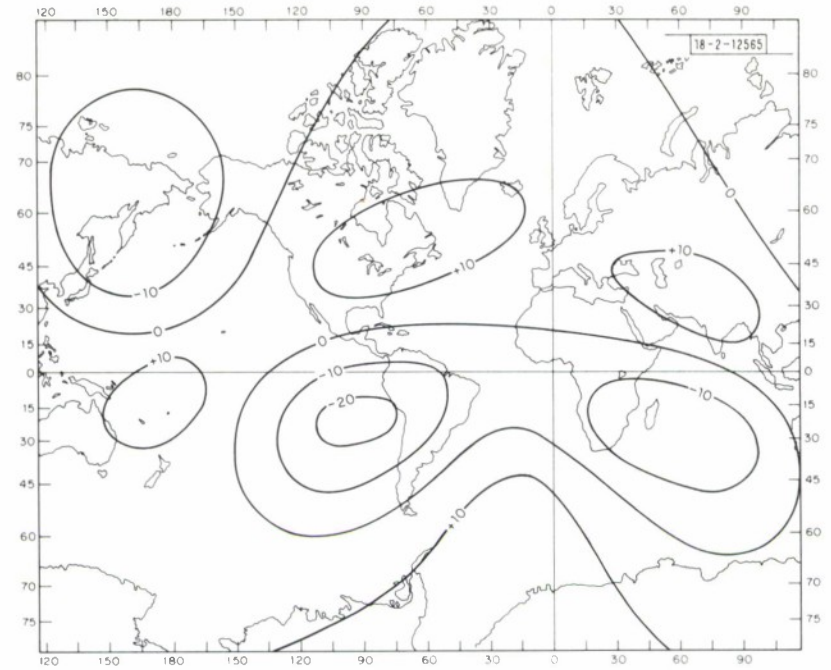

(c) Region III

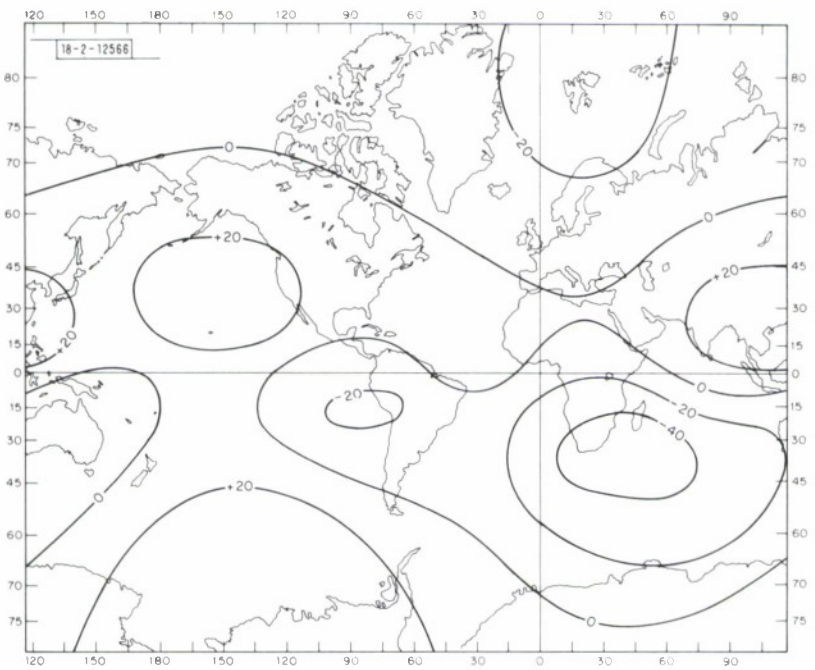

(d) Region IV

Fig. IV-1(a-d). Continued.

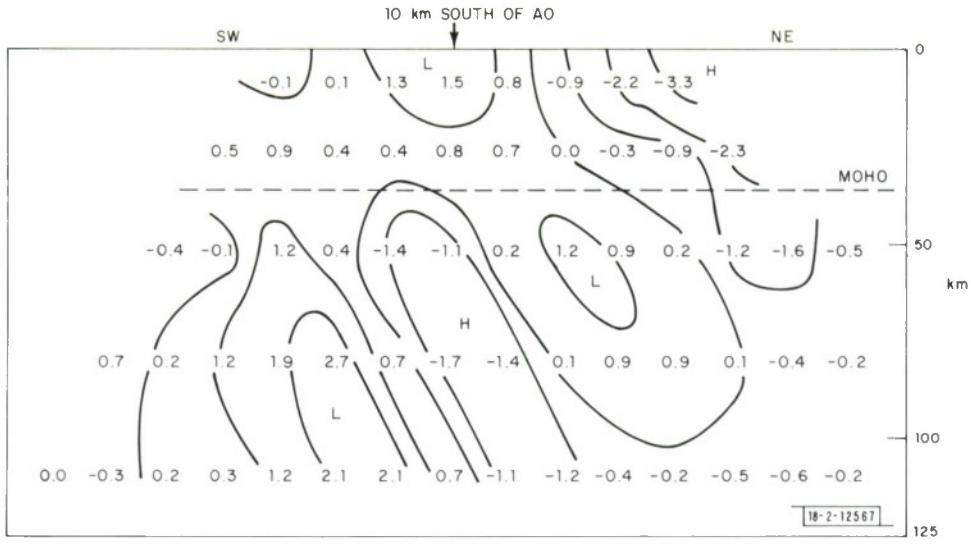

Fig. IV-2. NORSAR SW-NE cross section 10 km south of A0.

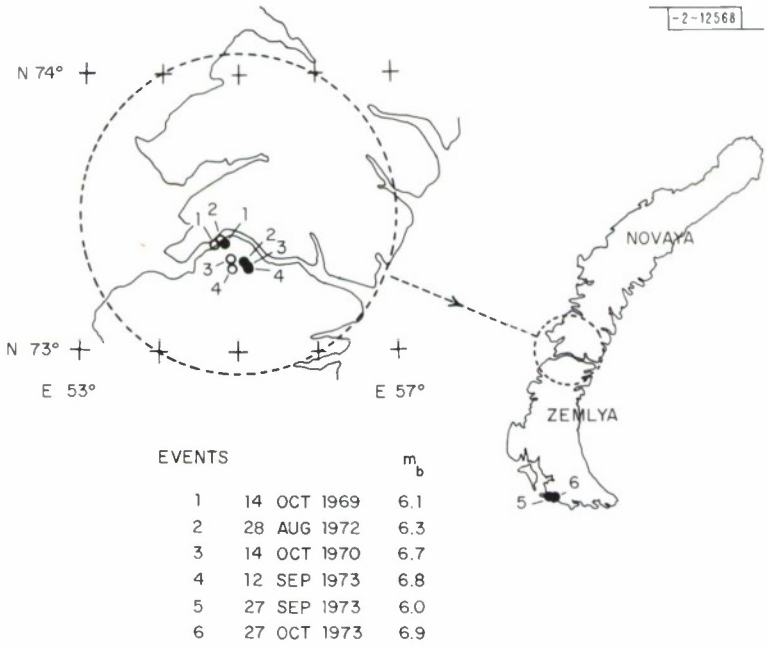

Fig. IV-3. Map of Novaya Zemlya showing locations of six presumed explosions. Black circles are PDE locations, and open circles are four relocated epicenters using 19 WWSSN stations.

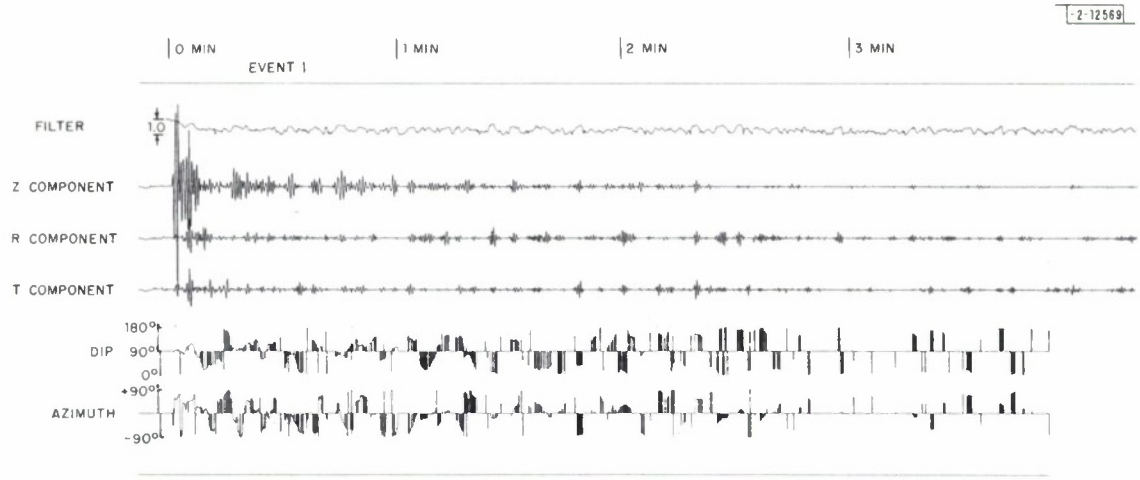

Fig. IV-4. Three-component data for Event 1. Above unfiltered data is polarization gain which equals 1 if data are linearly polarized, and 0 if circularly polarized. Polarized data equal principal component of data projected onto data and scaled by polarization gain.

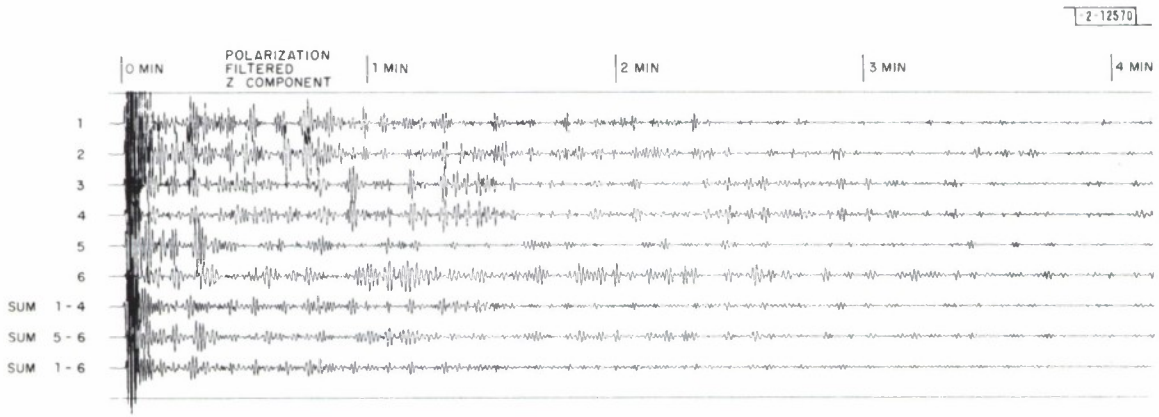

Fig. IV-5. Z components of six events, each polarized and normalized to $m_b = 6.5$. Also shown is sum of Events 1 to 4, sum of Events 5 and 6, and sum of Events 1 to 6.

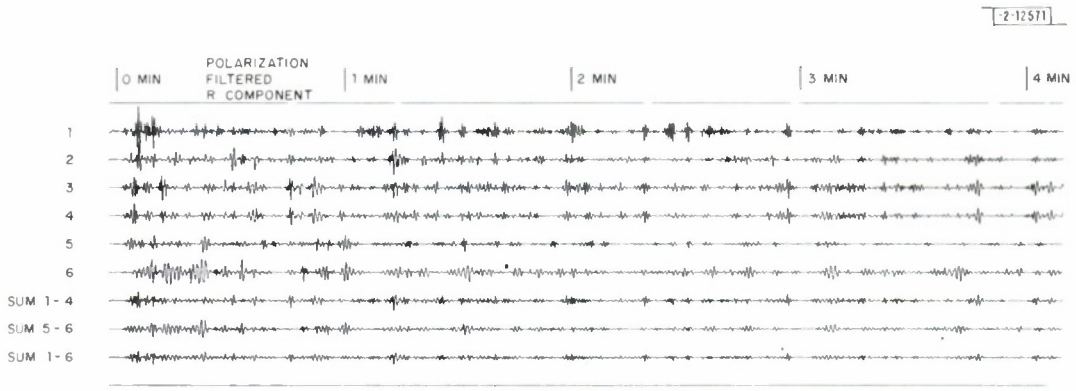

Fig. IV-6. R components of six events, each polarized and normalized to m_b = 6.5.

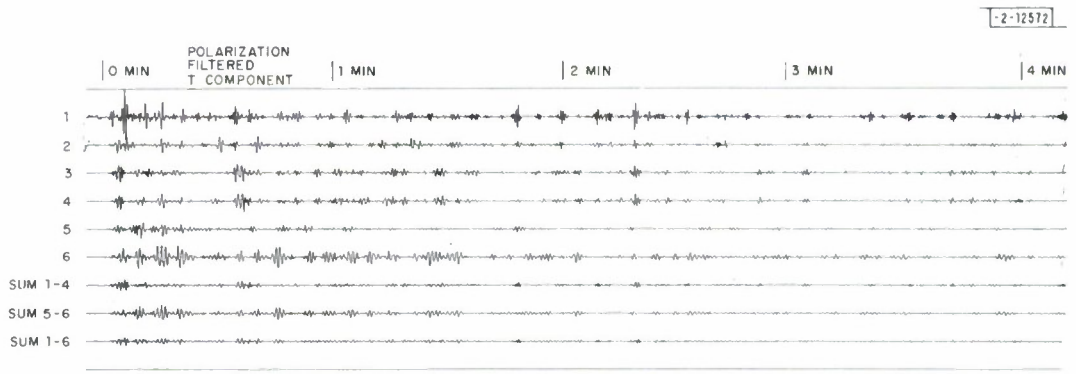

Fig. IV-7. T components of six events, each polarized and normalized to m_b = 6.5.

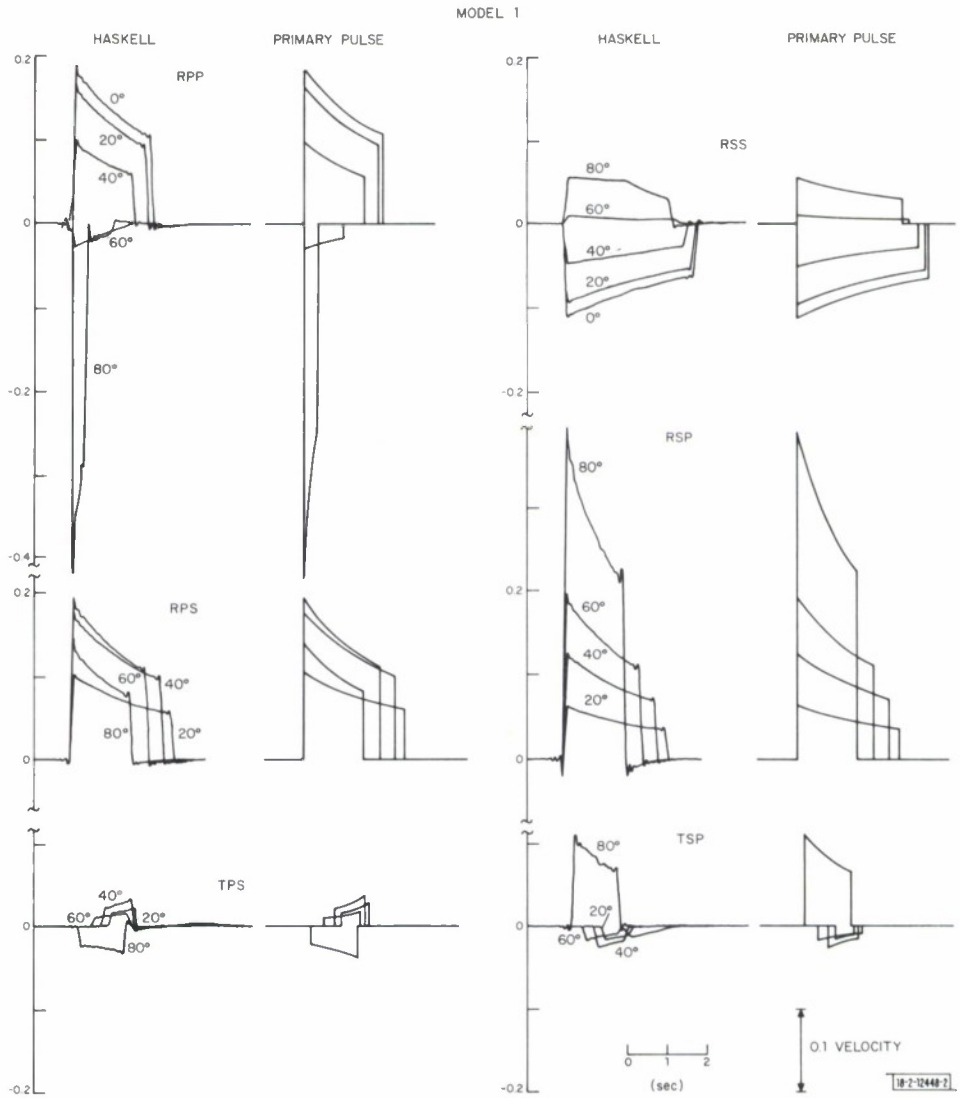

Fig. IV-8. Time domain reflection and transmission responses for Model 1. Each response is computed by Haskell's method and primary-pulse method, which are displayed side by side. All angles are incident P-wave angles. SV incident waves have same slowness as given P-angle in each response.

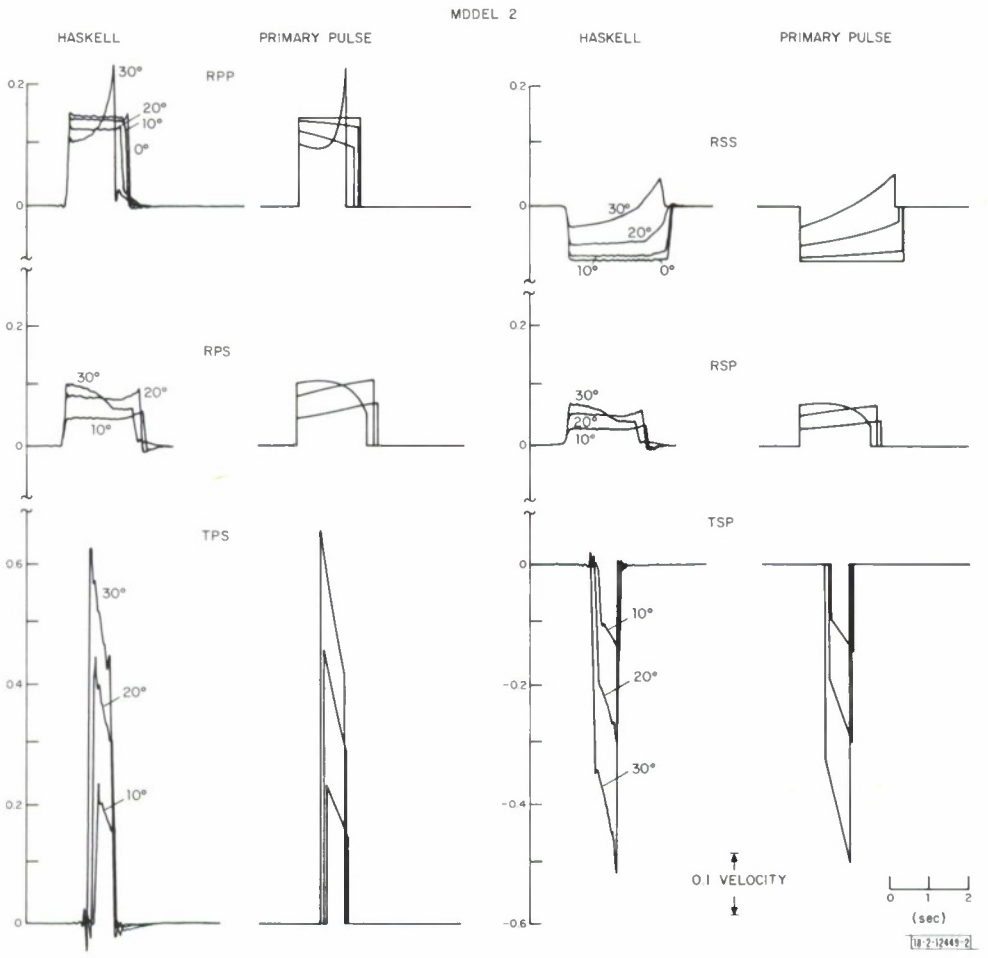

Fig. IV-9. Time domain reflection and transmission responses for Model 2. As in Fig. IV-8, all angles displayed are P-wave incident angles.

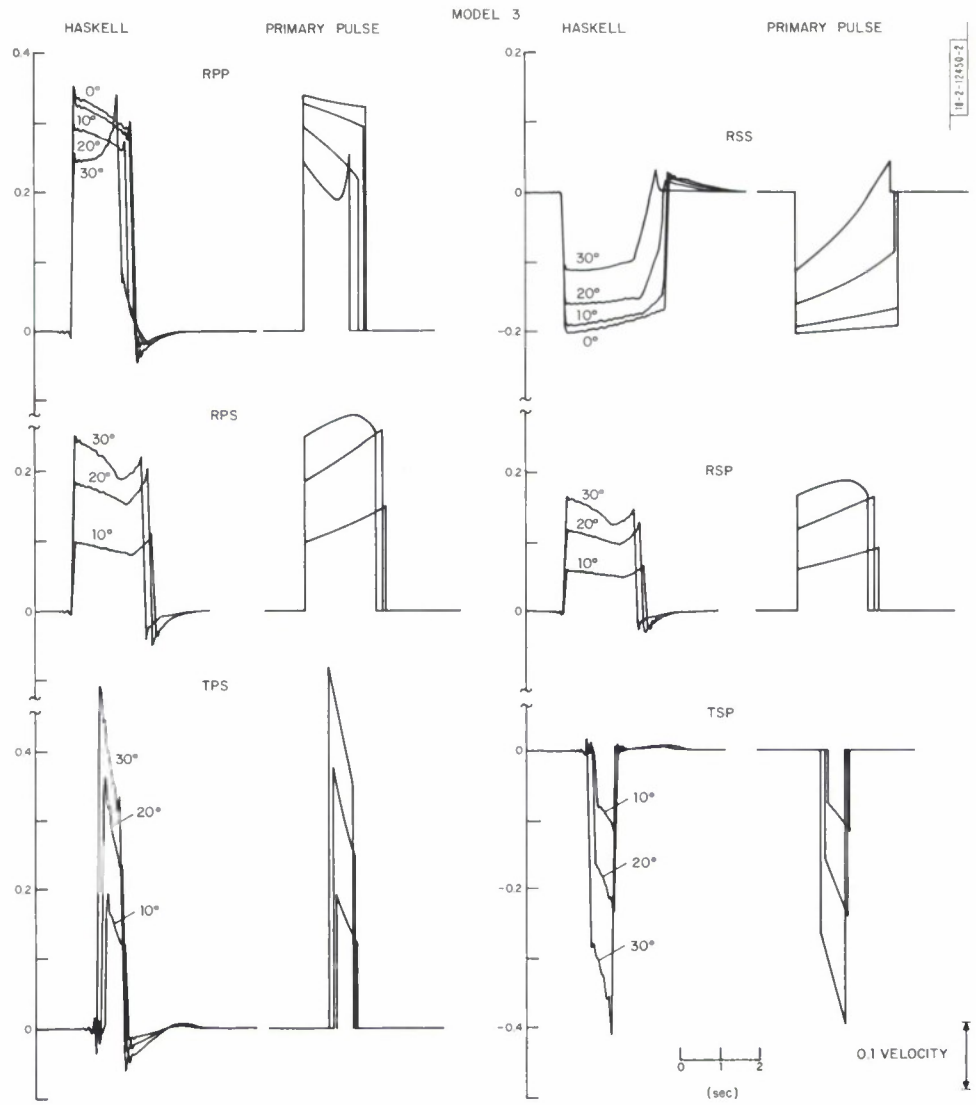

Fig. IV-10. Time domain reflection and transmission responses for Model 3. All angles are incident P-wave angles.

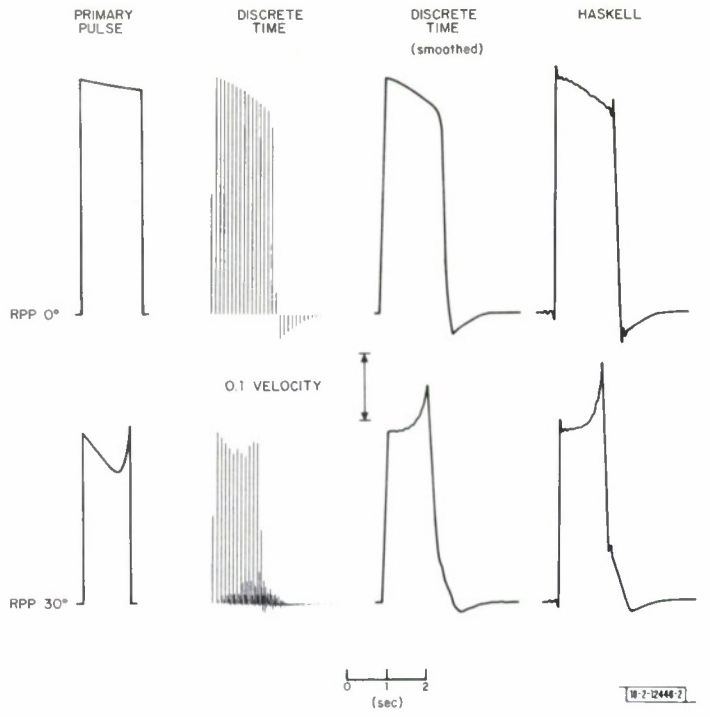

Fig. IV-11. Time domain reflection responses RPP for Model 3 calculated by three different methods for normal incidence and near critical incidence. Smoothed discrete time method is obtained by convolving unsmoothed response with a triangular kernel of area 1.

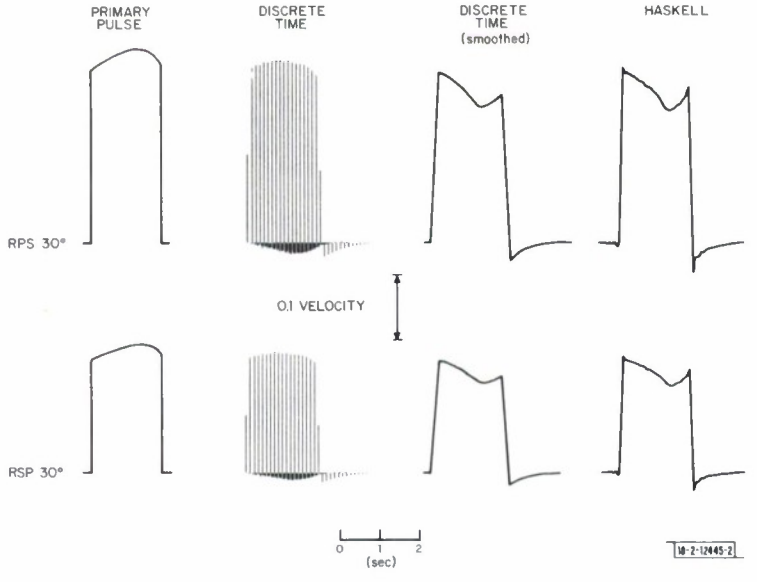

Fig. IV-12. Time domain reflection responses RPS and RSP for Model 3 at near critical incident angles. Angles given are P-wave.

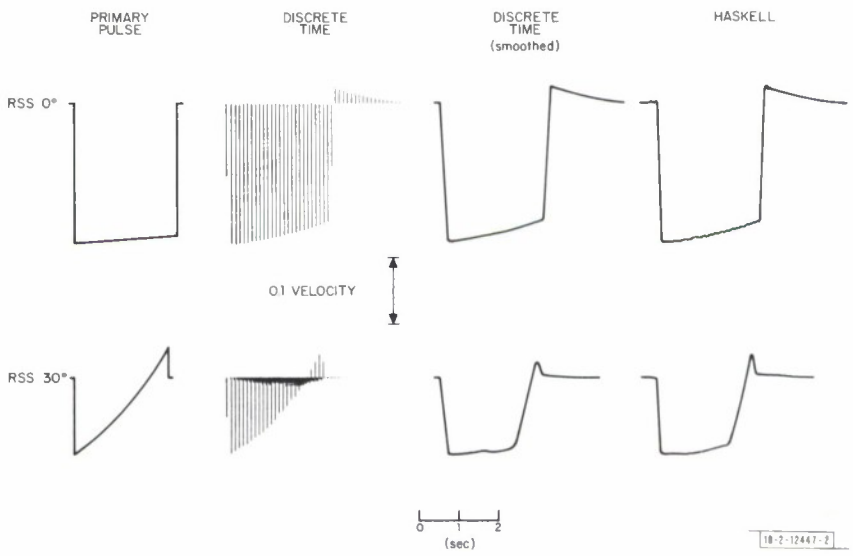

Fig. IV-13. Time domain reflection response RSS for Model 3 at normal and near critical incident angles. Angles given are for P-waves of same slowness as incident SV-waves.

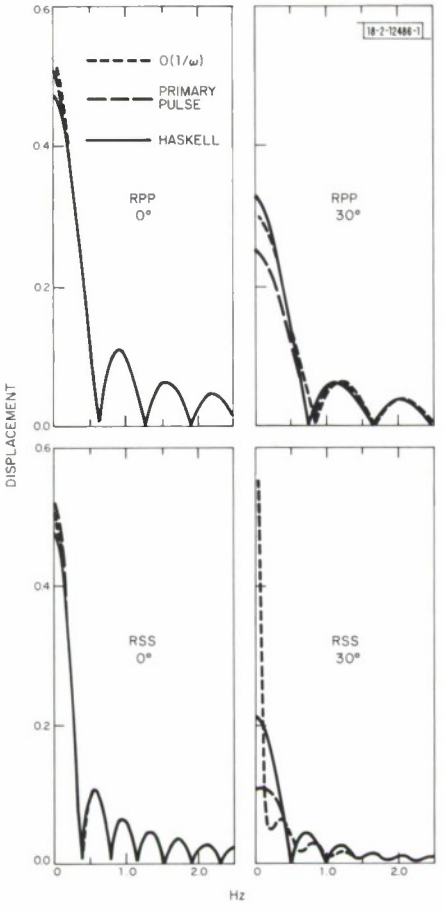

Fig. IV-14. Frequency domain responses RPP and RSS for Model 3 at normal and near critical angles of incidence. Each $0(1/\omega)$ response is spectrum of time domain discontinuities at beginning and end of primary pulse response.

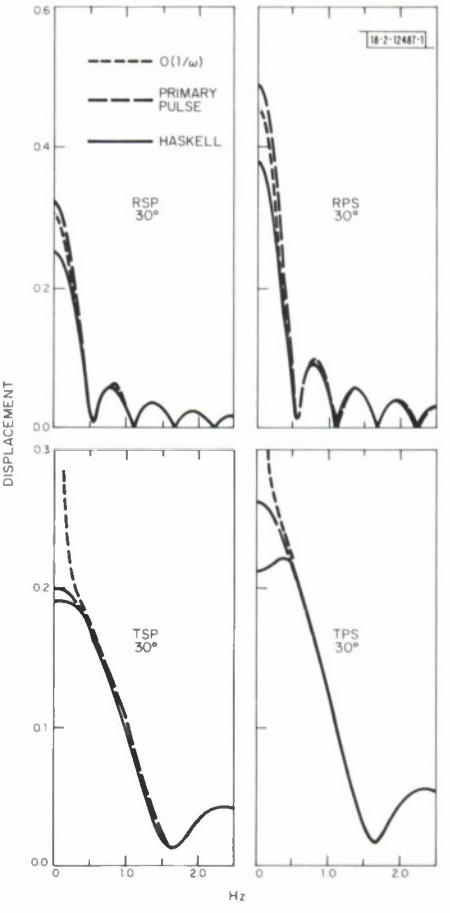

Fig. IV-15. Frequency domain responses RPS, RSP, TPS, and TSP at near critical angle of incidence to Model 3. Each $0(1/\omega)$ response is spectrum of two time domain discontinuities in primary pulse shape.

V. EARTHQUAKE OCCURRENCE RATES

A. SPATIAL AND TEMPORAL VARIATIONS IN THE FREQUENCY-MAGNITUDE CURVE

Spatial variations in the level of the frequency-magnitude curve are well known, and in Secs. B and C below, the temporal variations in this level are discussed. First, however, we shall examine evidence for changes in the shape of the curve in space and time. In spite of a voluminous literature, the evidence that these changes in shape occur is still very questionable.[1]

The detection of spatial variations in shape is confused by differences in the definition of magnitude, and by network detection characteristics (which are a strong function of location at lower magnitudes). If they are real, spatial variations should be readily apparent in the NEIS PDE catalog, which has a good global detection threshold and a reasonably consistent measure of magnitude m_b.

Data from this catalog for the period 1964.0 to 1974.3 have been subdivided on the basis of seismic region number into three broad tectonic types: subduction zones, oceanic ridge and transform areas, and shield areas. Frequency-magnitude curves for these three regimes are shown in Fig. V-1. In spite of the large differences in level, these curves match one another very closely, except for inevitable scatter at high magnitudes where there are very few events.

A representation of these types of data that recently has been introduced is the b-m_b plot. The maximum-likelihood estimate of the slope b of a straight line fitted to the data is given by[2]

$$b = \frac{0.4343}{\overline{M} - M_{min}}$$

where $\overline{M}$ is the average magnitude of all the events considered, and M_{min} is the lower threshold of magnitude used. Clearly, an estimate of b can be made for various different thresholds, and then b can be plotted against threshold.

Figure V-2 shows such plots for the three tectonic environments. 95-percent confidence limits on each point may be calculated as $\pm 1.96\, b/\sqrt{n}$, where n is the number of events used. The differences between these curves are not significant at the 95-percent level. Notice, however, that all three depart significantly from linearity.

We have concluded from these results, and from similar data from smaller regions, that the 10 years of data in the PDE listing do not indicate significant variations in space of the shape of the frequency-magnitude curve. Studies in the literature that appear to show otherwise (e.g., Acharya[3]) may be entirely the result of failing to take account of the spatial variation in network detection threshold.

Temporal variations in the shape of the frequency-magnitude curve have received less attention in the literature. We show one example from the PDE catalog that argues against these variations on a time scale of years. Figure V-3 shows the frequency-magnitude curve for the Northwest Pacific during the activity maximum of 1964-65, and for the period 1966-74, both normalized to events per year. The differences between the shape of these curves are not significant. This result makes an interesting comparison with those described in Sec. B below.

M. A. Chinnery

B. CORRELATIONS BETWEEN SEISMIC ACTIVITY IN WIDELY SEPARATED REGIONS

The Lincoln Laboratory Data Analysis and Display System (DADS)[4] is a powerful tool for the examination of tabular data. With the aid of this system, we have carried out a number of investigations of the characteristics of earthquake catalogs. The present study compares temporal variations in the level of seismic activity between different areas.

The principal source of data for this study is the NEIS PDE catalog. This listing appears to have been relatively homogeneous since 1964, and we have therefore used this list for the period 1 January 1964 to 30 April 1974. Supplementing this, we have the Regional Catalogue of Earthquakes published by the Japan Meteorological Agency (January 1964 to January 1970), the list[5] of earthquakes in the Southern California region published by the California Institute of Technology (January 1964 to December 1971), and the Bulletin of the International Seismological Center (January 1964 to December 1970).

These catalogs were used to construct earthquake time series for a number of regions, selected on the basis of seismic region number. These time series consist of counts of earthquakes per unit time with magnitudes greater than or equal to a given threshold. Thresholds were chosen so that reasonably complete counts could be expected. In the case of the PDE listing, earthquakes smaller than $m_b = 5.2$ were not used.

Data shown in the present study are obtained from counts over 40-day intervals. An example of one such histogram is shown in Fig. V-4(a) for shallow subduction zone earthquakes bordering the Pacific Ocean. The time series constructed in this way contain a considerable amount of high-frequency "noise," and the character of the time series becomes clearer after smoothing. We have applied a sliding 200-day window to the data, and the result is shown in Fig. V-4(b).

The activity maximum in 1965 is only partially the result of the Alaskan earthquake and the Rat Island sequence. A similar graph [Fig. V-4(c)] for deep earthquakes (depth > 300 km) also shows a maximum during 1965. In both cases, the maximum is a factor of 4 or 5 higher than the subsequent lows in mid-1966 and mid-1967, and a factor of about 2 higher than the mean for the whole period.

Time series have been constructed for a number of smaller regions of the globe, and 12 of these are shown in Figs. V-5 and V-6. All regions show an activity maximum during 1965, followed by minima in mid-1966 and mid-1967. The location of the 1965 peak varies considerably with region, but this may be a local phenomenon, since the subsequent minima show much less variation. After 1968, the correlation between the time series is much less impressive.

These data are interpreted as a first indication of the presence of a global triggering stress that fluctuates rapidly. Stress release by large earthquakes will normally occur near peaks of the triggering stress, when a region is very close to failure. When the local stress is not close to failure, variations in the applied stress appear to be reflected in the numbers of small- to medium-size earthquakes that occur. This suggests that information about the nature of the triggering stress may be obtained from earthquake time series.

Detailed study of these time series is continuing. Their spectral characteristics are discussed in Sec. C below.

M. A. Chinnery
T. E. Landers

C. SPECTRA FROM TWO MONTHS TO TWO YEARS OF REGIONAL EARTHQUAKE OCCURRENCE RATES

In a previous SATS,[6] the level of seismic activity (events per magnitude interval) was shown to be a time-dependent function independent of the magnitude range over which it is determined. Consequently, the spectrum of the corresponding seismic occurrence rate function (events within a magnitude range per time interval) for global seismicity data was examined and found to have a significantly nonrandom concentration of power at a period near 230 days.[7] The energy contained in this spectral peak amounted to approximately one-third of the total energy in the spectrum. To determine whether this periodicity is a global phenomenon of all seismic regions or peculiar to certain tectonic regions, the spectra of the earthquake occurrence rate sequences for various tectonic areas were computed. In addition, the resolution of the maximum entropy spectral analysis[7] was increased to determine if other less-powerful nonrandom spectral peaks were present.

The following is a list of zones considered.

(1) The entire shallow (depth $\leqslant$ 100 km) Pacific (Regions 1 to 301).[8]

(2) The entire nonshallow Pacific.

(3) The entire shallow Atlantic (Regions 402 to 414).

(4) Shallow India-Tibet-Szechwan-Yunan (Regions 302 to 319).

(5) Shallow Western Asia-Middle East-Crimea-Balkans-Western Mediterranean (Regions 347 to 401).

(6) The following Pacific zones, all shallow:

  (a) Alaska-Aleutian Arc (Regions 1 to 17)

  (b) Mexico-Guatemala Area-Central America-Caribbean Loop-Andean South America (Regions 53 to 146)

  (c) Kermadec-Tonga-Samoa Area-Fiji Islands Area (Regions 169 to 182)

  (d) New Hebrides Islands-Bismark and Solomon Islands-New Guinea-Caroline Islands to Guam (Regions 183 to 210).

  (e) Japan-Kuriles-Kamchatka (Regions 217 to 230)

  (f) Philippines-Borneo-Celebes-Sunda Arc-Burma-Southeast Asia (Regions 248 to 301).

The data source was the PDE, and the time span was 1964 to the present.

The sequences were prepared in the following manner. To prevent aliasing, daily sum data were lowpassed with a 3-pole Butterworth filter with a 3-dB cutoff at 1/(40 days), and then sampled at 20- or 10-day intervals. To preserve the phase, the filter was passed first forward and then reversed and the data truncated at both ends at twice the impulse response of the filter. In a similar manner, the data were highpassed above 1/(2 years). The resulting sequences were then analyzed using the Burg Maximum Entropy Method (BMEM).[9]

The most-critical and least-understood parameter in computing a spectrum using the BMEM is the filter length. The use of a filter with a length greater than the order of the process can result in spurious peaks. A shorter filter can diminish the resolution. Filter lengths comparable to the number of data points for high-order processes can bias the spectrum. Ulrych and Bishop[9] discuss these problems and present an approximate method to estimate the filter length. Accordingly, filters one-quarter the length of the data were used. The prediction error vs filter length curves for these data were computed, and indicated that for this length the spectra should not contain any spurious peaks but that some peaks may not be resolved. This situation, rather than the reverse, is judged preferable for this type of study since it is desired to correlate spectral peaks that do not dominate the spectra.

Figure V-7 shows the results for the shallow Pacific data. The total 1964-74 sequence was divided into three equal nonoverlapping time segments, and the Burg prediction error filter and the corresponding spectrum were computed for each section. The spectrum for each segment shows a peak near 235 days. Other peaks, even though containing considerable energy, are only characteristic of individual segments and so imply a rather large degree of nonstationarity in time in the complete sequence. The peak at 235 days contains approximately 30 percent of the spectral energy, determined by integrating the spectra.

The largest peak in the spectrum of solid earth tides in the band considered here occurs at 6 months.[10] Peaks at 6 months and 1 year dominate the spectrum of the rate of change of the earth's rotation.[11] To examine if these periodicities were present in the occurrence rate of earthquakes, spectra were computed on the whole sequences using a corresponding longer filter length (and consequently higher resolving power) so that if peaks at 182 days and 365 days exist, then they would be resolved from the peak at 235 days. Figure V-8 gives the spectra for the Pacific and Atlantic sequences. As well as the 235-day peak, a peak at 6 months is present in both sequences. The results for all ten shallow sequences show that the 6-month peak is the only peak observed in every spectra. The mean value is 181.8 days, with a standard deviation of 5.4 days. This peak on average contains about 5 percent of the total energy of the spectra. No consistent yearly peaks are observed. The peak near 235 days occurs for all sequences for regions bordering the Pacific Plate and the Atlantic Ridge. The mean value is 231.3 days, and the standard deviation is 18.1 days. These peaks contain an average of 15 percent of the total energy and are always one of the four largest peaks in the spectrum in which they occur. Figure V-9 shows the spectra in the two zones outside the Pacific and Atlantic areas. The 6-month peak is both time and space stationary for these regions; it accounts for approximately 20 percent of the energy in the spectrum of the occurrence rate in the Western Mediterranean to China seismic zone, and for about 5 percent of the energy for the shallow Pacific and Atlantic sequences.

In summary, in the band 2 months to 2 years, approximately one-third of the energy in the earthquake occurrence rate spectrum is time and space stationary, nonrandom, and periodic. For continental seismicity, the period is 6 months. For oceanic seismicity, the period is near 235 days (approximately 7.6 months) with a smaller amount of energy at a period of 6 months. No coherent energy at a period of 1 year is observed for either the oceanic or continental seismic occurrence rates.

T. E. Landers

REFERENCES

1. S. Shlien and M. N. Toksoz, "Frequency-Magnitude Statistics of Earthquake Occurrences," Earthquake Notes 41, 5 (1970).
2. K. Aki, "Maximum Likelihood Estimate of b in the Formula log N = a − bM and Its Confidence Limits," Bull. Earthquake Res. Inst., Tokyo Univ. 43, 237 (1965).
3. H. Acharya, "Magnitude-Frequency Relation and Deep-Focus Earthquakes," Bull. Seismol. Soc. Am. 61, 1345 (1971).
4. Seismic Discrimination SATS, Lincoln Laboratory, M.I.T. (30 June 1973), DDC AD-766559/9.
5. J. A. Hileman, C. R. Allen, and J. M. Nordquist, "Seismicity of the Southern California Region 1 January 1932 to 31 December 1972," published by Seismological Laboratory, California Institute of Technology (1973).
6. Seismic Discrimination SATS, Lincoln Laboratory, M.I.T. (30 June 1974), DDC AD-785377/3.
7. Loc. cit. (31 December 1974), DDC AD-A006194/5.
8. E. A. Flinn, E. R. Engdahl, and A. R. Hill, "Seismic and Geographical Regionalization," Bull. Seismol. Soc. Am. 64, 771-992 (1974).
9. T. J. Ulrych and T. N. Bishop, "Maximum Entropy Spectral Analysis and Autoregressive Decomposition," Rev. Geophys. and Space Phys. 13, 183-200 (1975).
10. P. Melchoir, "Harmonic Analysis of Earth Tides," in Methods in Computational Physics, Vol. 13 (Academic Press, New York, 1973), pp. 271-343.
11. K. Lambeck and A. Cazenave, "The Earth's Rotation and Atmospheric Circulation – I. Seasonal Variations," J. R. Astron. Soc. 32, 79-93 (1973).

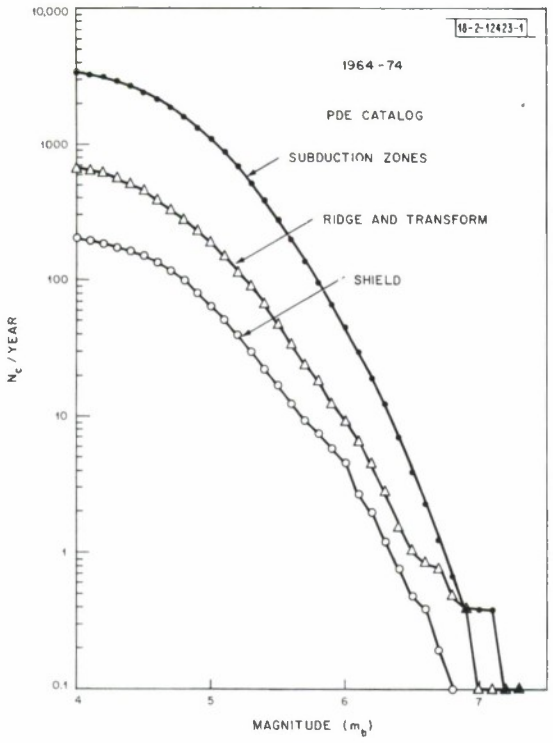

Fig. V-1. Frequency-magnitude curves for three tectonic environments

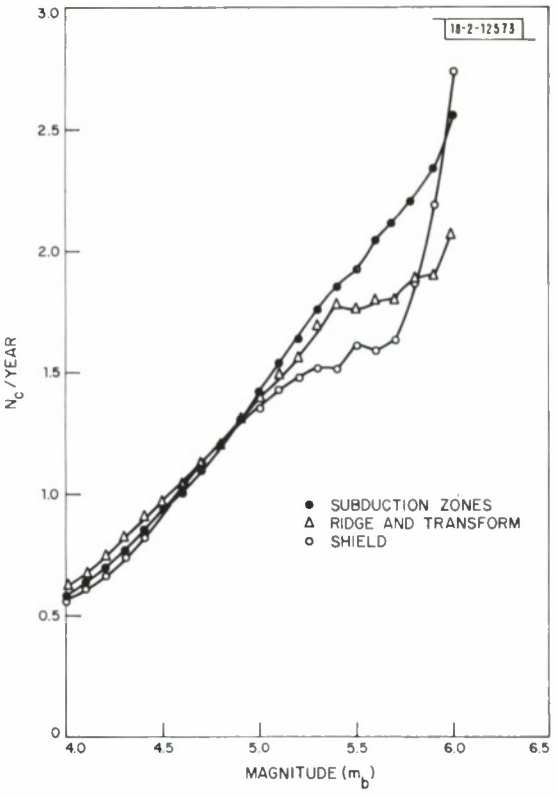

Fig. V-2. b-m_b plots for three curves in Fig. V-1.

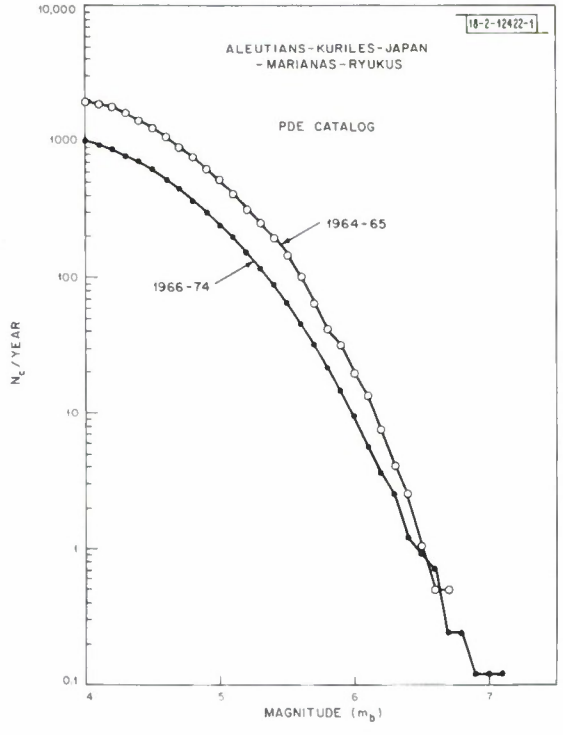

Fig. V-3. Comparison of frequency-magnitude curves for Northwest Pacific for activity maximum of 1964-65 and period 1966-74.

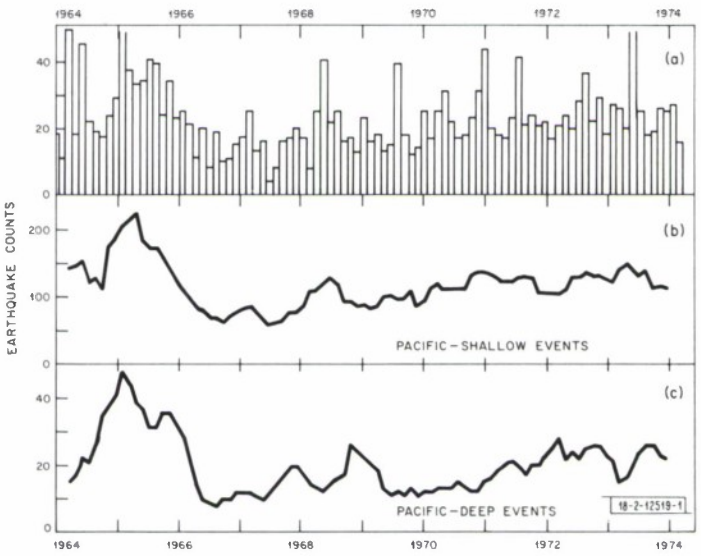

Fig. V-4. Earthquake time series for margins of Pacific Ocean. PDE catalog. (a) Histogram of earthquake counts for 40-day intervals (depth $\leqslant$ 100 km, $m_b \geqslant 5.5$); (b) same, smoothed by sliding 200-day window; and (c) smoothed time series for deep events (depth $\geqslant$ 300 km, $m_b \geqslant 5.2$).

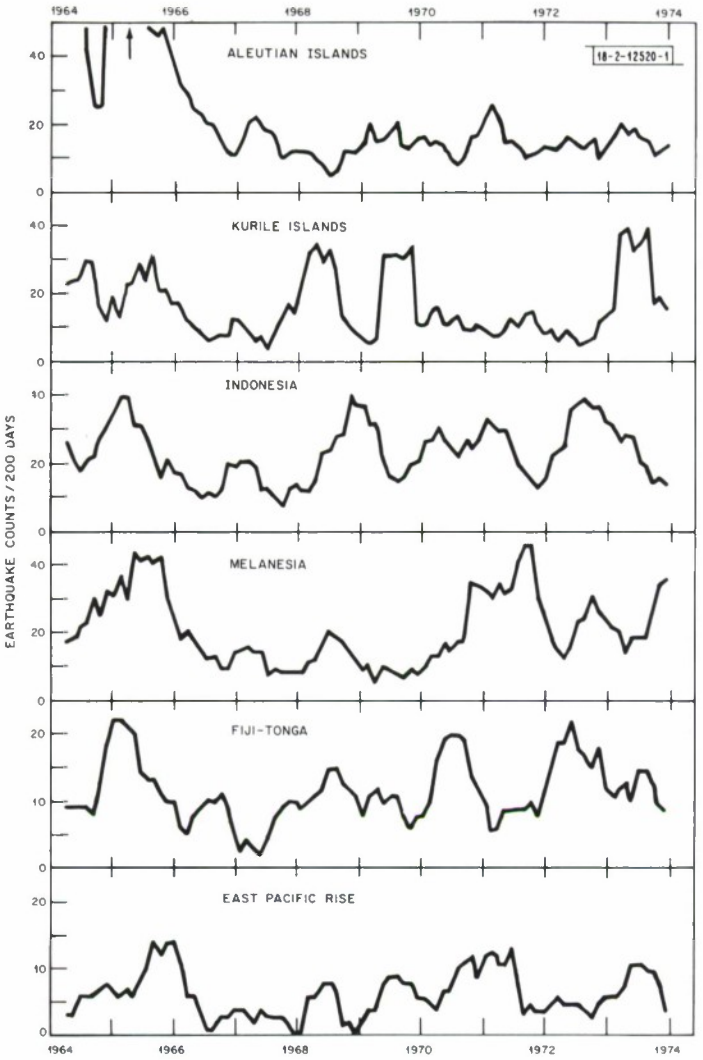

Fig. V-5. Time series for shallow (depth $\leq$ 100 km) events from regions bordering Pacific Plate, smoothed by 200-day sliding window. PDE catalog. Magnitude thresholds vary from m_b = 5.2 to 5.6.

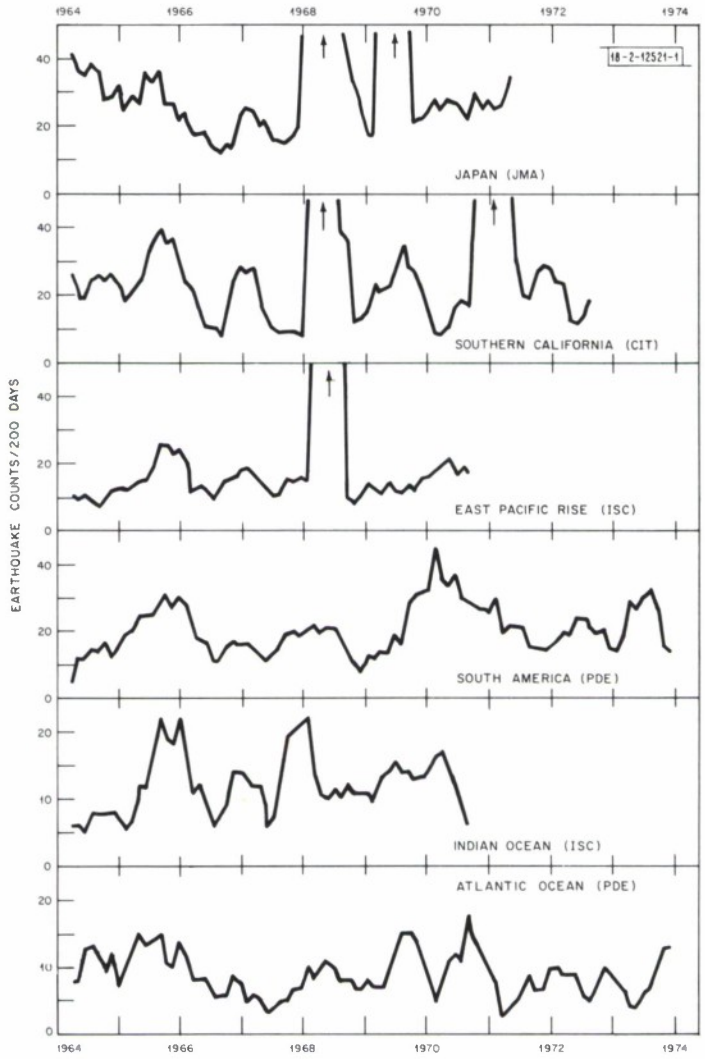

Fig. V-6. Time series for shallow (depth $\leqslant$ 100 km) events from several regions. Various catalogs (see text). Thresholds used are Japan (M = 5.2), Southern California (M_L = 3.5), East Pacific Rise (m_b = 4.8), South America (m_b = 5.4), Indian Ocean (m_b = 4.8), and Atlantic Ocean (m_b = 5.2).

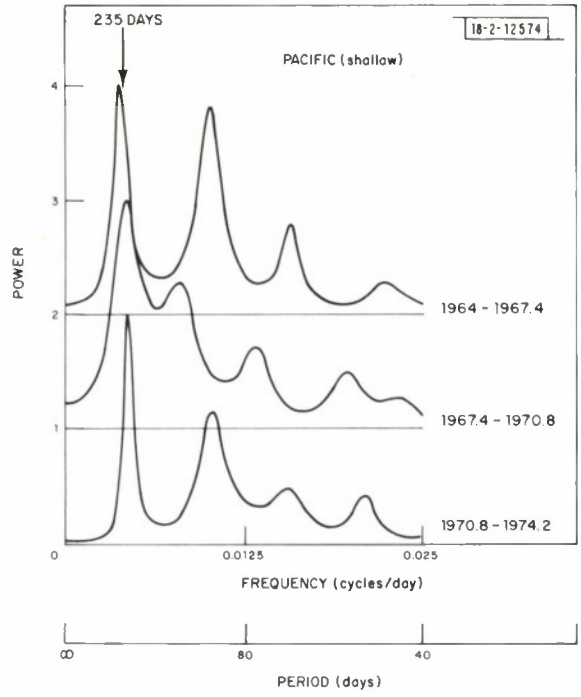

Fig. V-7. Spectra for three nonoverlapping time periods of data set 1, entire shallow Pacific. Earth section has strong peak near 235 days.

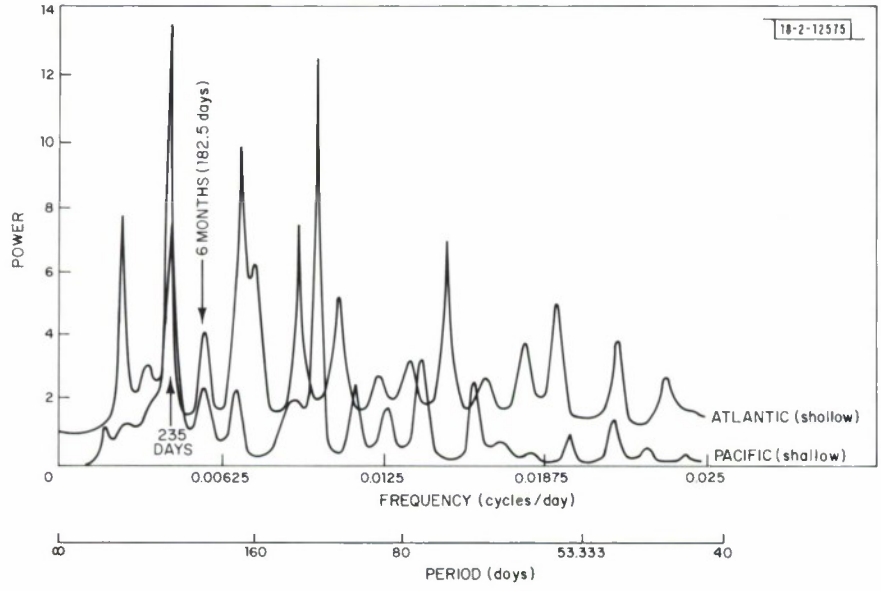

Fig. V-8. Spectra for data sets 1 and 3 showing that Atlantic and Pacific have global spectral peak near 235 days individually, and consistent 6-month peak.

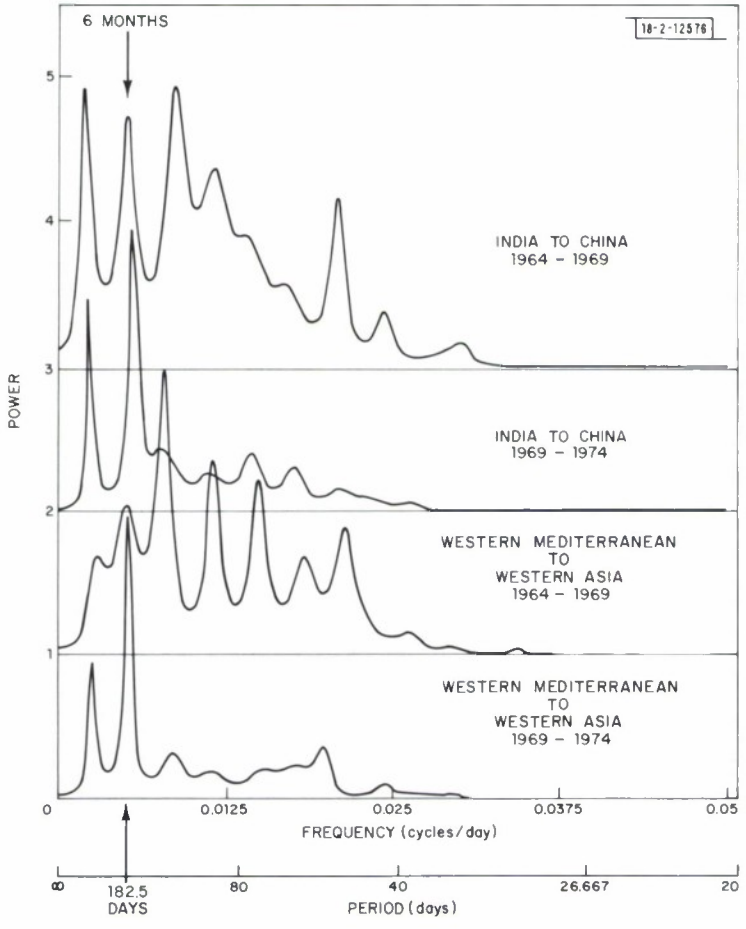

Fig. V-9. Spectra for sequences 4 and 5. Dominant period for Mediterranean through Southern Asia belt is 6 months.

VI. SEISMIC DATA MANAGEMENT AND COMPUTER SYSTEMS

A. SEISMIC DATA MANAGEMENT SYSTEM

Work is continuing within this system to develop file structures and contents which will accurately reflect the status of seismic data and information available from ARPA-supported seismic facilities. Because much of this system is still in the design and implementation stages, the major effort has been in setting up files and file structures which will eventually receive most of the information. The information already in existence for the more stable components of this system [such as the large arrays, the high-gain long-period (HGLP) sites, datacomputer, etc.] has been reduced and structured within NLS files (the On Line System developed by Stanford Research Institute). Most of the installation reports from the HGLP sites have been entered into files of NLS. These reports have been restructured to take advantage of the capabilities of the NLS. Also included in these files are the graphic plots for the seismometer response curves at each HGLP site. Generally, most of the available information on the HGLP sites is in the NLS. The one remaining piece of information to be included concerns the actual data tapes produced at each of the HGLP sites.

The situation with the seismic research observatories (SROs) is another matter. Because much of this program is still in the planning and implementation stages, only information on the observatory hardware and software systems is now in the NLS file system. This is possible because the hardware and software systems are nearly identical for each observatory. However, because many of the actual site locations are currently being negotiated, only those sites which are well along in their implementation and installation stages have been considered at this point. In the master file containing data on all components of the IWWSS, the individual SROs are described in detail. Each SRO exists as a separate branch within this file. Contained in this branch is information on the site geology, location, operations, and operator address. As more SROs become operational, each entry will be completed for that particular site.

Other files contained in the NLS system for IWWSS are continually being updated to reflect the progress of the total system. Some of the recent updates include the Datacomputer Datalanguage Manual 0/11. This manual is being entered into NLS, and at this time is almost complete. Having this manual located on-line and available for immediate reference should prove beneficial to users of the datacomputer, within the scope of the IWWSS.

R. M. Sheppard

B. DATACOMPUTER ACCESS EXPERIMENT

One of the major components in the IWWSS is the datacomputer at Computer Corporation of America (CCA). This data-storage computer will serve as the filing system and storage device for the real seismic data, as well as for processed data such as bulletins, site status, etc. One important question which we feel needs investigation concerns the access time to a reasonably large data base stored in this datacomputer. One of the many files that will eventually be stored in this computer will be an event bulletin file. This file will probably become large within a short time after it is created. Access to such a large file and performing conditional searches on this file could become a time-consuming process. At this point, we are attempting to obtain some idea of what the access time and search times will be on a file which may reasonably represent the bulletin file.

In an attempt to produce a file which will have some resemblance to the bulletin file, we have organized an epicenter bulletin list from both the USGS epicenter list and the daily bulletins of both NORSAR and LASA. Combining these bulletin lists for the period 1900 to mid-1974 has produced a bulletin file of over 113,000 events. With the help of CCA personnel, the bulletin file has been stored in the datacomputer. Access to this bulletin file is obtained through the program "SMART," written by personnel at CCA and runable at most TENEX sites. This program is being used as a means of checking on access time into this large epicenter bulletin data file.

The initial use of SMART was to check on the accuracy of the stored data. Simple data checks were performed to see if the data for various parameters fell within logical ranges. For example, SMART was used to check the event depth for values <0 or >850. In this manner, each event parameter field was checked to determine the initial success in accurately storing the seismic data. In the complete file of over 113,000 events, only 3 events were found to be erroneous.

During the initial check on access time with SMART, the performance of a simple check on a single field took upwards of 19 min. elapsed time and 30 sec of CPU time. These figures varied considerably, from 11 min. upwards to 19 min. for access and search time. Some weeks later, the same data search took from 2 to 4 min. Since the program SMART is being run at Office-1 on the ARPANET and is checking on data stored at the datacomputer at CCA, many factors must be considered in the analysis of the datacomputer access time across the ARPANET. More detailed checks are now being performed on this epicenter file and the across time required to use such a large data base.

R. M. Sheppard

C. THE ASG ARPANET CONNECTION

The Applied Seismology Group (ASG) uses the Lincoln Laboratory IBM 370/168 as its main computer resource for heavy number crunching and interactive data processing. Normal access to the system would be via IBM 2741 terminals. These are slow (15 cps) and cannot handle graphics. To improve the situation, the ASG has bought two Tektronix 4014-1 Graphics Display Terminals. These are run at 4800 baud (480 cps). Rather than use leased lines, the connection to the Lincoln Laboratory machine is via the ARPANET, a network of heterogeneous computers. In addition to giving us the desired high-speed connections to Lincoln, it lets us access the other sites with ease. We are already using it to access the NLS at Office-1 where all the information about the IWWSS is maintained, and the datacomputer at CCA which will at some point contain a large seismic base.

All our terminals (two 4014's, two TI silent 700's, and a Datapoint) are connected to a PDP-11/50 at our Carleton Street site. This, in turn, is connected via a special interface to the network. On the 11/50 we run the ELF software system to support the various network protocols. In the current configuration, it can support up to 6 terminals simultaneously (at present we have only 5 terminals). Reliability is tolerable for an interim system: 3 crashes/day on 4 days out of 5; 10 crashes on the fifth day.

In addition to providing terminal access to the ARPANET, the system allows the users to get listings from the remote site and print them locally. This facility is used heavily from various TENEX sites (Office-1, BBN, etc.).

We also have a PDP-11/40 with 64K core. Hardware reconfiguration enabling the 11/40 to run ELF is under way. When completed, we will be able to run more users and have room to

insert software to handle specific ASG problems. The 11/50 will then be free for program development and direct support of seismic data processing.

Y. Peduel

D. PDP-7 CONSOLE EXPANSION

As our research effort emphasis goes from a few large arrays to networks of stations, certain limitations of the Seismic Data Analysis Console† and of the data formats which it can use have become apparent. We have therefore undertaken modifications and software development which will allow us to use the Console system more effectively with seismograms from a network of stations. This will allow us to utilize the power and features of the Console for network data without developing a completely new system for the purpose.

The planned changes to the Console are:

(1) Modify the CRT display to show more identification information for individual traces. This has been completed.

(2) Allow the user to operate a knob to time-shift a single seismic trace on the display without changing other displayed traces, and to selectively change the gain of individual traces. The required software changes to achieve this have been identified, and coding is in progress.

(3) Provide for efficient event-oriented initialization of the Console from a new format data tape containing network seismograms. In addition to the seismogram itself, the new tape format will contain all station and instrument information required by the initialization program for each seismogram. The structure of the Console system will allow us to write the new initialization capability in Fortran once a small number of assembly language programs are written. Neither the design nor assembly language subroutines are currently completed.

(4) Provide for dumping the data of a Console session, including station identification, instrument, and time information for each individual channel, on tape for future processing. A simple program to do this has been written. It generates a tape which subsequently can be used to re-initialize the Console with a single command. With some minor modifications this is sufficient for the immediate future, but eventually the capability to output in a more standard form for use by other programs will be required.

The new format input tapes to the Console mentioned above will be quite general and not just limited to Console application. They will contain four distinct sections, namely: (1) Type, (2) Description, (3) Title, and (4) Body. The four of these together will constitute a Data Unit (DU). The Body of a DU will contain actual data. What is stored, how it is stored, and how it can be manipulated are determined by the Type and Description sections. The Description section will specify the logical structure of the data items in the Body, while the Type section will specify the storage device and the physical representation of the items. The Title will be

† P. L. Fleck and L. J. Turek, "A Seismic Data Analysis Console," Technical Report 495, Lincoln Laboratory, M.I.T. (18 January 1972), DDC AD-740604.

a short section containing creation date and some alphanumeric text supplied by the user to help him identify the data in the DU. A program using a DU must first check the Type and Description to determine whether it can handle that DU. The representation of the Type and Description sections is a function of the storage device containing the DU. Thus, when a DU is accessed we know automatically how to read these sections because we know what device we are using.

Our first planned use of Data Units is to input multi-site waveform data to the Console. In particular, the SROs and HGLP stations are of interest. Such data will be input to the Console via a single family of DUs which have a common Description. The Description will specify that the Body is a stream of objects, each object consisting of a header giving start times, station name, etc., and an array of waveform samples. Although not specified by the Description, the objects will be ordered according to the start times. Long waveforms, say more than a thousand samples, will simply be broken into a number of objects. The Console initialization program will work from a condition table listing the station, instrument, and time intervals of interest, and then scan through the DU transferring to the Console all data that satisfy the given conditions. This approach gives great flexibility in the way the user can request data, since the condition table can be set up in a variety of ways. For example, suppose an initialization program to get short-period P-wave data based upon predicted P-arrival times for an event is required but does not exist. It will be necessary only to write a Fortran program to create a condition table containing the computed arrival times at the stations of interest.

A program is being written to convert a single 9-track SRO tape into a DU on a 7-track tape which can be read by the PDP-7 computers which support the Console. In addition, a program to merge DUs from different stations on the basis of signal start times is being written. This merge is required to obtain a library of DU tapes with all network data for a time period on a single tape. This can be done routinely and means that subsequent Console users generally will need to mount only one tape to get all available data for an event.

R. T. Lacoss
L. J. Turek
M. F. O'Brien

E. SOFTWARE LIBRARIES

Seismic research activities are aided considerably by general and application program libraries which are adequately documented and easy to use. In the past we have developed, and we continue to expand, a very extensive library for our PDP-7 computers. This library is on-line and always available to users and programs. In addition, a smaller library has been maintained for batch processing on the Lincoln IBM 370/168. This has been limited largely to routines to read data tapes and to perform functions such as high-resolution spectral analysis which require considerable computing power.

Our ARPANET connection to the Lincoln 370/168 has enhanced our access to that facility and its utility to us. To make the best use of this, we have undertaken to significantly expand and reorganize our program libraries on that system. Although some of this will involve changes in the library available for batch processing, the major effort is directed toward a new library for interactive use.

Work on the new library for time-sharing users of the IBM 370/168 has just been started. The first stage is primarily the conversion of existing programs and generation of proper documentation for their use in the new environment. Since many programs actually are interfaces

to data bases such as names and locations of seismic stations, travel-time curves, and digitized maps, the new library will contain such data as well as actual programs. A routine to obtain seismic station locations from their names is now available. Other basic routines currently available to users on our PDP-7 systems will be added shortly.

R. M. Sheppard
L. Lande

REPORT DOCUMENTATION PAGE		READ INSTRUCTIONS BEFORE COMPLETING FORM
1. REPORT NUMBER ESD-TR-75-205	2. GOVT ACCESSION NO.	3. RECIPIENT'S CATALOG NUMBER
4. TITLE *(and Subtitle)* Seismic Discrimination		5. TYPE OF REPORT & PERIOD COVERED Semiannual Technical Summary, 1 January – 30 June 1975
		6. PERFORMING ORG. REPORT NUMBER
7. AUTHOR*(s)* Chinnery, Michael A.		8. CONTRACT OR GRANT NUMBER*(s)* F19628-73-C-0002
9. PERFORMING ORGANIZATION NAME AND ADDRESS Lincoln Laboratory, M.I.T. P.O. Box 73 Lexington, MA 02173		10. PROGRAM ELEMENT, PROJECT, TASK AREA & WORK UNIT NUMBERS ARPA Order 512 Program Element No. 62701E
11. CONTROLLING OFFICE NAME AND ADDRESS Advanced Research Projects Agency 1400 Wilson Boulevard Arlington, VA 22209		12. REPORT DATE 30 June 1975
		13. NUMBER OF PAGES 82
14. MONITORING AGENCY NAME & ADDRESS *(if different from Controlling Office)* Electronic Systems Division Hanscom AFB Bedford, MA 01731		15. SECURITY CLASS. *(of this report)* Unclassified
		15a. DECLASSIFICATION DOWNGRADING SCHEDULE

16. DISTRIBUTION STATEMENT *(of this Report)*

Approved for public release; distribution unlimited.

17. DISTRIBUTION STATEMENT *(of the abstract entered in Block 20, if different from Report)*

18. SUPPLEMENTARY NOTES

None

19. KEY WORDS *(Continue on reverse side if necessary and identify by block number)*

seismic discrimination	surface waves	NORSAR
seismic array	LASA	ARPANET
seismology	body waves	

20. ABSTRACT *(Continue on reverse side if necessary and identify by block number)*

This report describes 23 investigations in the field of seismic discrimination. These are grouped as follows: seismic body wave studies (3 contributions), seismic surface wave studies (5 contributions), investigations of seismic source mechanisms (2 contributions), studies of earth heterogeneity and scattering phenomena (5 contributions), studies of earthquake occurrence rates (3 contributions), and outlines of progress in seismic data management system development and improvements in in-house computer facilities (5 contributions).

☆U.S. GOVERNMENT PRINTING OFFICE: 1975—A-0298/(42) 7